Recharge and source-water insights from the Galapagos Islands using noble gases and stable isotopes

Rohit B. Warrier,[1] Maria Clara Castro,[1] and Chris M. Hall[1]

Received 21 May 2011; revised 1 December 2011; accepted 14 January 2012; published 8 March 2012.

[1] Through a combined noble gas and stable isotope study carried out in the Galapagos Islands of Santa Cruz and San Cristobal, we demonstrate the utility of atmospheric noble gases in identifying recharge areas and timing of recharge in fractured, basaltic systems. Timing of recharge obtained through noble gas temperatures (NGTs) for all samples is corroborated by stable isotopes. Except for one sample, combined NGTs and stable isotope analyses point to recharge during the hot season for all low-altitude ($<\sim$420 m) spring samples from San Cristobal and all basal aquifer samples in Santa Cruz. Stable isotope comparisons also indicate that San Cristobal springs located at high altitudes (>420 m above sea level) are recharged during both the "garúa" and hot seasons. Preservation of seasonality independently recorded by NGTs and stable isotopes is further reinforced by estimated young water ages. Samples located at high-altitude display systematic deviations of dissolved noble gases from expected air saturated water values and lead to inconsistent recharge altitudes and temperatures using standard NGT models. Existing degassing models are unable to account for the observed noble gas pattern for most samples. We explore various mechanisms to assess their potential at reproducing the observed noble gas signature. In particular, the potential impact of fog droplets during the cooler "garúa" season on dissolved noble gas concentrations in groundwater and the effect of mixing high-altitude ($\geq$1500 m) rainwater with low-altitude ($\sim$400 m) fog droplets is explored. This mixing hypothesis is capable of explaining Ne and Xe concentrations for most high-altitude samples.

Citation: Warrier, R. B., M. C. Castro, and C. M. Hall (2012), Recharge and source-water insights from the Galapagos Islands using noble gases and stable isotopes, *Water Resour. Res.*, *48*, W03508, doi:10.1029/2011WR010954.

1. Introduction

[2] Among the numerous applications of noble gas geochemistry, the study of noble gases (He, Ne, Ar, Kr, and Xe) dissolved in groundwater can enhance our understanding of surface and groundwater dynamics by providing us with indications about flow paths, connectivity between aquifers, and water residence times [e.g., *Andrews and Lee*, 1979; *Andrews et al.*, 1982; *Bottomley et al.*, 1984; *Torgersen and Ivey*, 1985; *Stute et al.*, 1992; *Castro et al.*, 1998a, 1998b; *Bethke et al.*, 1999; *Castro et al.*, 2005, 2007]. In addition, because Ne, Ar, Kr, and Xe are conservative tracers and their concentrations in the recharge areas of groundwater systems are typically considered to be simply a function of temperature (T), pressure (P) (altitude of recharge area), salinity (S), and excess air (A), noble gas temperatures (NGTs) have commonly been regarded as a potentially robust indicator of past climate [e.g., *Stute and Schlosser*, 1993; *Kipfer et al.*, 2002; *Sun et al.*, 2010].

[3] For over four decades, noble gas studies in groundwater have been carried out extensively in sedimentary systems. However, to this day, few studies have been conducted in volcanic, fractured groundwater flow systems. These include the Cascades Volcanic Arc [*James et al.*, 2000; *Saar et al.*, 2005], Yellowstone [*Mazor and Fournier*, 1973; *Mazor*, 1977; *Kennedy et al.*, 1985, 1988; *Lowenstern and Hurwitz*, 2008; *Gardner et al.*, 2010], Cape Verde Islands [*Heilweil et al.*, 2009], the Azores archipelago [*Jean-Baptiste et al.*, 2009], and the Reunion [*Marty et al.*, 1993]. So far, however, none of these studies has taken advantage of information provided by NGTs. Unlike the islands of Santa Cruz and San Cristobal in the Galapagos, in which no volcanic and/or hydrothermal activity is present, most of these volcanic systems are extremely active and thus, are not comparable to our study area. Volcanic systems and equatorial and tropical basaltic islands in particular, typically have complex internal structures and challenging access, are often poorly characterized with respect to groundwater resources and frequently suffer from freshwater scarcity and/or groundwater contamination problems. The Galapagos Archipelago, a UNESCO World Heritage site, famous for its unique fauna and flora, is one example of such a region, and has historically been regarded as an inhospitable land due to a lack of this vital resource [e.g., *d'Ozouville*, 2007]. Development of a comprehensive long-term freshwater exploitation and management plan will ensure preservation of natural habitats while

[1]Department of Earth and Environmental Sciences, University of Michigan, Ann Arbor, Michigan, USA.

0043-1397/12/2011WR010954

providing the required potable water needs for the island's inhabitants. Such an exploitation and management plan requires an in depth and overall understanding of the hydrogeology of these islands [e.g., *Adelinet et al.*, 2008; *d'Ozouville et al.*, 2008a; *d'Ozouville et al.*, 2008b; *Auken et al.*, 2009]. Two critical aspects to achieving such a goal are the identification of recharge areas as well as the timing of recharge, currently unknown in these systems.

[4] Noble gases have previously been used to provide constraints on recharge locations and/or timing of recharge in different systems [e.g., *Aeschbach-Hertig et al.*, 1999; *Manning and Solomon*, 2003]. Because many basaltic islands present a steep altitude gradient and thus, a steep temperature gradient, in addition to having a climate characterized by two distinct seasons with markedly distinct average temperature and precipitation values, the atmospheric component of Ne, Ar, Kr, and Xe is expected to provide constraints on both recharge locations and timing of recharge in these systems. This last decade has seen a surge of studies dedicated to improving NGT estimation techniques as well as studies aimed at better understanding the behavior of noble gases in the unsaturated zone and at the water table/soil air interface in sedimentary systems [*Mercury et al.*, 2003, 2004, *Peeters et al.*, 2002, *Hall et al.*, 2005; *Castro et al.*, 2007; *Aeschbach-Hertig et al.*, 2008; *Cey et al.*, 2008; *Sun et al.*, 2008; *Cey et al.*, 2009; *Sun et al.*, 2010]. All these recent studies have led to an in depth level of understanding of physical processes in sedimentary systems capable of affecting the atmospheric component of noble gases and thus, estimated NGTs, far greater than previously achieved. Similar studies in basaltic areas, however, have not yet been carried out.

[5] Here, through a combined noble gas and stable isotope study carried out in the Galapagos Islands of Santa Cruz and San Cristobal, we demonstrate the utility of atmospheric noble gases at identifying recharge areas and timing of recharge in basaltic systems, while providing specific answers with respect to recharge location, timing of recharge and groundwater residence times in these islands. Simultaneously, we highlight the need to conduct further in depth noble gas studies in fractured and basaltic regions in particular, to enhance our understanding of processes capable of impacting NGTs in these systems and, in particular, capable of leading to the unexpected relative Ar excess and simultaneous depletion of Ne, Kr, and Xe observed in a number of our samples.

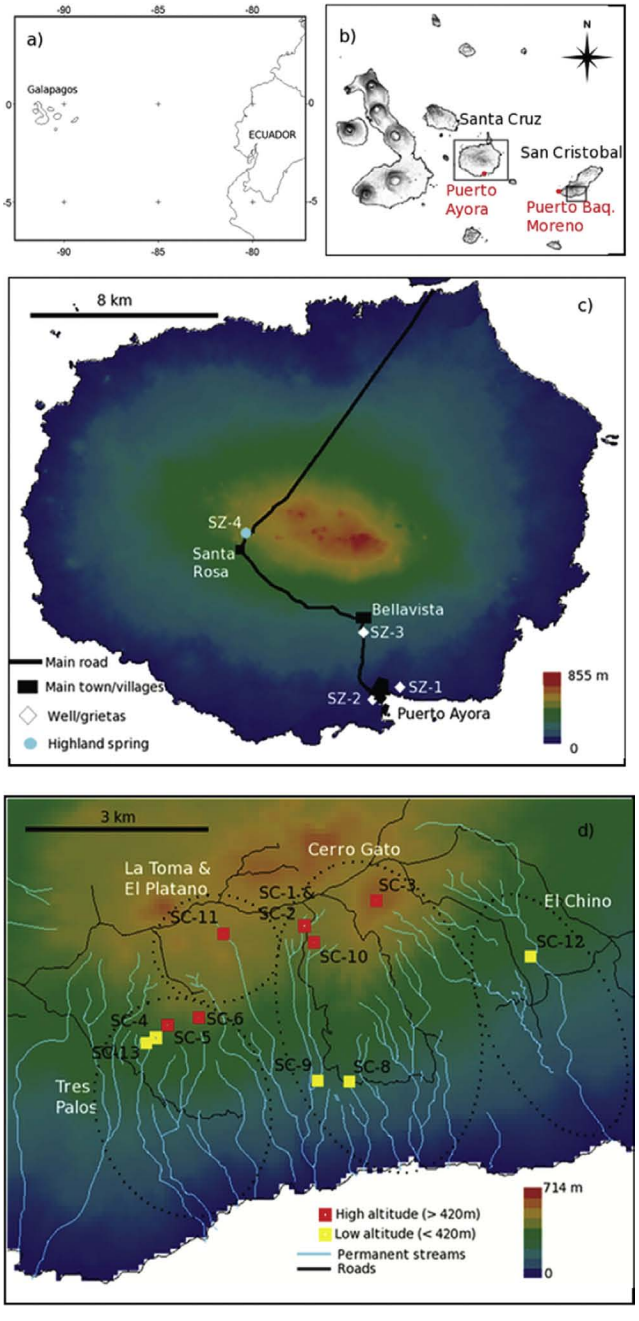

Figure 1. (a) Location of Galapagos Islands off the coast of Ecuador; (b) location of Santa Cruz and San Cristobal islands and the main inhabited towns; (c) Santa Cruz Island elevation from SRTM (Shuttle Radar Topography Mission) [*d'Ozouville et al.*, 2008b] data and sampled locations are indicated; (d) San Cristobal Island elevation from SRTM data and location of spring sample (southern windward slope) are indicated. Springs are distinguished as high (>420 m) versus low altitude (<420 m).

2. Geological, Hydrogeological, and Climate Regional Settings

[6] The Galapagos Islands, located on the equator in the eastern Pacific Ocean, about 1000 km off the coast of Ecuador (Figures 1a and 1b) emerge from a shallow submarine platform which forms the western part of the East-West trending Carnegie Ridge on the Nazca plate [e.g., *Geist et al.*, 1988; *White et al.*, 1993]. Santa Cruz and San Cristobal (Figure 1b), two of the oldest islands (~1.3 Ma and ~2.35 Ma, respectively) [*Geist et al.*, 1986; *White et al.* 1993], are located in the central and eastern most portion of the archipelago. Although *White et al.* [1993] comment that Santa Cruz and San Cristobal can both be considered (theoretically) active, so far as we know, neither has erupted in the past 10,000 years. Also, neither has an active geothermal system, and the youngest basalts on both are very primitive, making a shallow magma body unlikely [*Geist et al.*, 1986]. In practice, both islands can be considered inactive (L. Siebert and T. Simkin, Volcanoes of the world: An illustrated catalog of holocene volcanoes and their eruptions,

available online at http://www.volcano.si.edu/world, 2002; D. J. Geist, personal communication, 2011).

[7] Studies of Santa Cruz and San Cristobal hydrogeological systems have recently intensified, with generation of digital elevation models, field based hydrological instrumentation, as well as extensive coverage by helicopter-borne electromagnetic prospecting [*d'Ozouville*, 2007; *d'Ozouville et al.*, 2008a; *d'Ozouville et al.*, 2008b; *Auken et al.*, 2009]. These studies identified: (1) a basal aquifer, which appears to be continuous, surrounds the islands and penetrates at least 9 km inland; and (2) perched aquifers on the southern, windward portion of both islands. Unlike San Cristobal, direct access to the basal aquifer in Santa Cruz is possible through "grietas" (open fractures) in the vicinity of the coastline. The latter basal aquifer was also intercepted at a depth of ~160 m near Bellavista [*Proctor and Redfern International Limited*, 2003] (Figure 1c) and is now locally exploited. Only one perennial spring is known in Santa Cruz; it is the outlet of a small perched aquifer located in a volcanic cone at Santa Rosa. An extensive (50 km^2) continuous hidden perched aquifer with no visible outcrops was also identified in Santa Cruz, while a series of discontinuous perched aquifers leading to multiple water spring alignments and the presence of perennial streams was identified in San Cristobal (Figure 1d) [*d'Ozouville*, 2007; *d'Ozouville et al.*, 2008a]. The presence of a perennial hydrographic system is unique to San Cristobal. A perennial lake located in the crater of a volcanic cone, El Junco, is also found in San Cristobal at 690 m of elevation.

[8] Climate in the Galapagos Islands is characterized by a cool "garúa" season from June to December, and a rainy, hot season from January to May (Figure 2a) [*Trueman and d'Ozouville*, 2010]. Average "garúa" temperatures are 22.6 ± 3.4°C (see http://www.darwinfoundation.org/datazone/darwin_weather) and 23.5 ± 3.4°C (Figure 2; see http://www7.ncdc.noaa.gov/CDO/cdo) at sea level in Santa Cruz and San Cristobal, respectively. During the "garúa" season, a stable, inversion cloud layer is present between ~300 m and the summit of the islands (870 and 730 m, respectively, for Santa Cruz and San Cristobal) [*d'Ozouville*, 2007]. This stable inversion layer brings moisture laden mist to the upper portion of the islands. The hot, rainy season is characterized by short and intense episodes of precipitation (Figure 2a). Average temperatures during this season are 25.9 ± 2.0°C at sea level and 24.9 ± 1.5°C at 180 m in Santa Cruz (see http://www.darwinfoundation.org/datazone/darwin_weather) and 26.5 ± 2.7°C at sea level in San Cristobal (Figure 2; see http://www7.ncdc.noaa.gov/CDO/cdo). These distinct seasonal temperature variations yield an average annual temperature of 24.0 ± 3.9°C (see http://www.darwinfoundation.org/datazone/darwin_weather) and 24.8 ± 4.3°C (see http://www7.ncdc.

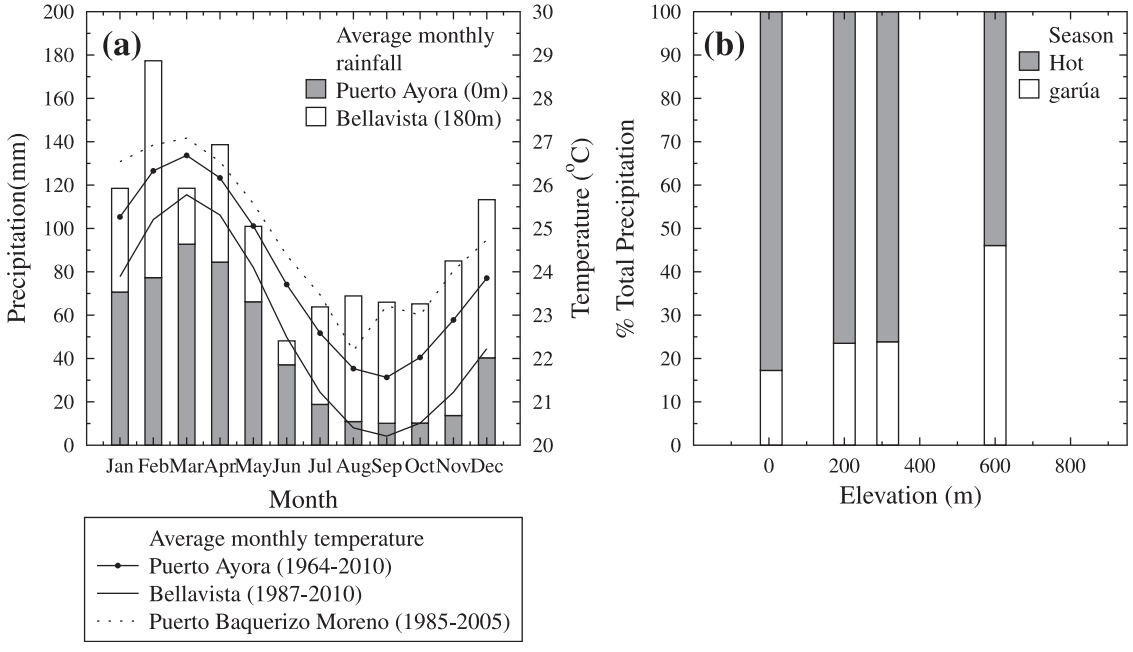

Figure 2. Meteorological information for Santa Cruz and San Cristobal (a) Monthly mean temperature and precipitation measurements from land weather stations located at Puerto Ayora (0 m asl) and Bellavista (180 m asl) in Santa Cruz, as well as Puerto Baquerizo Moreno (~0 m asl), in San Cristobal. Monthly mean temperatures are indicated and averaged over extended time periods for each station as available. Monthly average precipitations obtained for Puerto Ayora and Bellavista for the same time period are indicated as bars. Monthly average precipitation at sea level (solid gray bars) in Santa Cruz is less than that observed at Bellavista (solid white bars, 180 m) throughout the year. (b) Measured % contribution of precipitation during each season in 1969 at different altitudes in Santa Cruz. Percent contribution from the hot season (January–May) is indicated by gray bars while contribution from the "garúa" season (June–December) is indicated by white bars. Percent contribution from the "garúa" season increases with altitude increase.

noaa.gov/CDO/cdo) at sea level in Santa Cruz and San Cristobal, respectively.

[9] In addition to seasonal variations in temperature and precipitation, temperature and precipitation also vary as a function of altitude. While annual average temperatures vary with a gradient of −0.8°C/100 m [*d'Ozouville*, 2007] in Santa Cruz, average annual rainfall increases with altitude increase (see, e.g., Figure 2a). Precipitation-altitude patterns also indicate a greater contribution of "garúa" precipitation to the total annual precipitation with increasing altitude (Figure 2b). Indeed, while precipitation during the "garúa" season represents only ∼17% of total annual precipitation at an elevation of 6 m above sea level (asl), it accounts for up to 46% of total annual precipitation at an elevation of 600 m asl [*Kramer and Black*, 1970]. In addition, preliminary estimations point to a nonnegligible component of fog contribution to groundwater recharge during the "garúa" season at high altitude [*Dominguez et al.*, 2011]. A similar distribution of rainfall with altitude is observed in Santa Cruz [*d'Ozouville et al.*, 2008b]. While annual and monthly average temperatures and precipitations reflect available data over multiple years, large temperature and precipitation variations do occur from year to year. Such variations are particularly marked between El Nino and La Nina events [*d'Ozouville et al.*, 2008a] and need to be considered and discussed for comparison purposes.

3. Sampling and Analytic Methods

[10] 29 water samples were collected for analysis of noble gases at 16 different locations in Santa Cruz and San Cristobal in October 2007, on the windward (southward), inhabited portion of the islands (Figures 1c and 1d). These include six samples collected in Santa Cruz at four locations (Figure 1c), five samples in the basal aquifer, three near Puerto Ayora at sea level, and two near Bellavista, in addition to one sample collected from the spring of Santa Rosa. In addition, 23 samples were collected in San Cristobal at 12 locations (Figure 1d) of which 21 samples are from springs located in the El Chino, Cerro Gato, La Toma, El Platano and the Tres Palos watershed areas (∼200–570 m), and two samples are from the El Junco lake (690 m).

[11] All samples were analyzed for He, Ne, Ar, Kr and Xe in the Noble Gas Laboratory at the University of Michigan. Sampling and analytical procedures are briefly described below and can be found in more detail in the work of *Ma et al.* [2004], *Saar et al.* [2005], and *Castro et al.* [2009]. Water samples were also collected from each of the 16 sampling sites (Figures 1c and 1d) for measurement of δD and $\delta^{18}O$ in the Stable Isotope Laboratory at the University of Michigan following procedures described elsewhere [*Ma et al.*, 2004].

[12] Water samples for noble gas analyses were collected in copper tubes (i.e., standard refrigeration grade 3/8″ Cu tubing) and water was allowed to flow through for ∼10 min. While the water flushed through the system, absence of gas bubbles that could potentially contaminate or phase fractionate the samples was checked through a transparent plastic tube mounted at the end of the copper tube. Copper tubes were then sealed by stainless steel pinch-off clamps [*Weiss*, 1968]. The copper tubes were subsequently attached to a vacuum extraction system and noble gases were quantitatively extracted for inletting into a MAP-215 mass spectrometer. Noble gases were transported using water vapor as a carrier gas through two constrictions in the vacuum system, purified, and sequentially allowed to enter a MAP-215 mass spectrometer using a cryo-separator. The complete measurement procedure comprises measurement of He, Ne, Ar, Kr, and Xe concentrations, and their respective isotopic ratios, with standard errors for concentration measurements of 1.5, 1.3, 1.3, 1.5 and 2.2%, respectively. Noble gas concentrations are based on masses 4, 20, 36, 84 and 132 for He, Ne, Ar, Kr and Xe, respectively.

4. Results and Discussion

4.1. Noble Gas Patterns

[13] Sample names, location, altitude, water temperatures and electrical conductivity are provided in Table 1. Measured noble gas concentrations together with He and Ar isotopic ratios are given in Table 2. Noble gas concentrations in air saturated water (ASW) in equilibrium with the atmosphere for a temperature of 20°C and altitudes of 0 and 421 m, are also indicated for comparison. 421 m corresponds to the average altitude of all spring samples. Figure 3 shows all samples normalized to ASW at average sampling elevations of 0 m (basal aquifer) and 421 m (springs) for an average temperature of 20°C. This temperature value falls close to the range ($\pm 1\sigma$) of annual average temperature values at both sea level and 421 m in both islands. Annual average temperature values at 421 m were extrapolated from measured annual average temperatures at sea level in San Cristobal using the annual average temperature gradient of −0.8°C/100 m.

[14] Results show excess He and Ar concentrations in many samples from both the basal aquifer and springs with respect to ASW (Figure 3). He excesses in all basal aquifer samples range from 7 to 49% that of ASW, while He excesses of up to 22% are observed for most of the spring samples. The origin of these He excesses are constrained through measured R/R_a values (Table 2, where R is the measured $^3He/^4He$ ratio, and R_a is the atmospheric $^3He/^4He$ ratio of 1.384×10^{-6}) [*Clarke et al.*, 1976] and discussed below. Measured R/R_a for all spring samples vary between 0.095 ± 0.036 and 1.156 ± 0.082 while R/R_a for all basal aquifer samples vary between 1.176 ± 0.033 and 3.146 ± 0.075, respectively. In particular, measured R/R_a in as many as 13 out of 24 spring samples fall within $\pm 1\sigma$ error of the atmospheric value ($R/R_a = 1$), while the remaining 11 spring samples fall within $\pm 2\sigma$ error of the atmospheric value. Because R/Ra displays, for all spring samples, a value close to that of the atmospheric value ($R/R_a \approx 1$), the presence of a significant magmatic He component ($R/R_a \approx 8 \pm 1$) [*Farley and Neroda*, 1998] can be ruled out. Indeed, the slight He excesses observed in springs (∼0%–22%) can be readily explained by the addition of tritiogenic ^3He resulting from the β decay of natural and bomb ^3H [see e.g., *Schlosser et al.*, 1988, 1989]. Excess of tritiogenic ^3He in spring samples together with measured tritium concentrations in precipitation allows estimation of groundwater residence times for these springs (cf. section 6). By contrast, R/R_a for all basal aquifer samples (Santa Cruz) are significantly higher than the atmospheric value ($>\pm 2\sigma$) and point to the presence of a significant mantle component.

Table 1. Sample Numbers, Location, Altitude, Measured Water Temperature and Electrical Conductivity for All Samples

Sample No.	Latitude GWS.84 (South)	Longitude GWS.84 (West)	Altitude m (asl)	Electrical Conductivity $\mu S\ cm^{-1}$ at 25°C	Water Temperature (°C)
			Santa Cruz		
sz1-1[a]	0.738	90.302	0	8810	22.8
sz2-1[a]	0.7462	90.3194	0	4140	16
sz2-2[a]	〃	〃	0	4140	〃
sz3-1[a]	0.704	90.326	160	2550	22.5
sz3-2[a]	〃	〃	160	2550	〃
sz4-1	0.641	90.403	500	129	18.7
			San Cristobal		
sc1-1	0.9002	89.4919	519	96	18.2
sc1-2	〃	〃	519	96	〃
sc2-1	〃	〃	519	131	18.4
sc2-2	〃	〃	519	131	〃
sc3-1	0.896	89.48	690	30	19
sc3-2	〃	〃	690	30	〃
sc4-1	0.9172	89.5158	427	50	21.6
sc4-2	〃	〃	427	50	〃
sc5-1	0.9154	89.514	447	35	20.4
sc5-2	〃	〃	447	35	〃
sc6-1	0.9142	89.5089	463	57	18.8
sc6-2	〃	〃	463	57	〃
sc8-1	0.9241	89.4848	229	86	21.4
sc9-1	0.9238	89.4898	229	91	21.7
sc9-2	〃	〃	229	91	〃
sc10-1	0.9025	89.4904	417	38	20.3
sc10-2	〃	〃	417	38	〃
sc11-1	0.9012	89.505	572	39	21.2
sc11-2	〃	〃	572	39	〃
sc12-1	0.9048	89.4586	295	144	18.8
sc12-2	〃	〃	295	144	〃
sc13-1	0.9181	89.5174	382	75	21.8
sc13-2	〃	〃	382	75	〃

[a]Basal aquifer; With the exception of Lake El Junco (sc3-1, 3-2) and samples collected in the basal aquifer all other samples correspond to springs from perched aquifers.

He component separation analyses of the Santa Cruz basal aquifer samples (not shown) [see e.g., *Castro et al.*, 2000, *Castro*, 2004] indicates mantle He contributions between ~20% and ~70% with respect to total He excesses. The presence of a significant mantle He component in the basal aquifer and its simultaneous absence in springs from perched aquifers suggests that springs represent shallow groundwater with short residence times (cf. section 6) that are shielded by the influx of external mantle He by the deeper basal aquifer. Mantle He excesses in the basal aquifer samples will be discussed in detail elsewhere. Excess Ar concentrations of up to 14% (measurement precision is 1.3%) with respect to ASW are observed in spring samples. Measured $^{38}Ar/^{36}Ar$ and $^{40}Ar/^{36}Ar$ ratios (Table 2) for all samples (including basal aquifer samples) vary between 0.1882 ± 0.0041 and 0.1948 ± 0.0033 and 291.1 ± 0.94 and 297 ± 1.18, respectively. Ar isotopic ratios for all spring and basal aquifer samples are indistinguishable from ASW ($^{38}Ar/^{36}Ar = 0.1880$; $^{40}Ar/^{36}Ar = 295.5$) and indicate that the observed Ar excesses are of atmospheric origin. The presence of Ar excesses is discussed in detail below (section 7). While excesses are observed in He for most of the samples and Ar for many of the samples, the opposite is true for Ne, Kr, and Xe concentrations with most of the samples displaying a strong depletion with respect to ASW (Figure 3). While maximum observed Ne depletion with respect to ASW in springs and basal aquifer samples are 18% and 15%, respectively, a much stronger depletion of the heavier noble gases Kr and Xe is observed. Maximum Kr depletion of up to 32% and 18% and Xe depletion of up to 32% and 21% with respect to ASW are observed for springs and basal aquifer samples, respectively (Figure 3). While this stronger Kr and Xe depletion might be an artifact of the chosen ASW temperature, it is apparent from Figure 3 that Ne, Kr and Xe deviations from ASW values are systematic. Such systematic noble gas deviations from the expected ASW values cannot be due to atmospheric contamination during sampling or noble gas measurements. In particular, Ne concentrations dissolved in water would be expected to increase if air contamination had taken place [see e.g., *Kipfer et al.*, 2002]. In addition to the observed systematic Ne, Kr and Xe depletion for a significant subset of samples, multiple samples (e.g., Sc5-1, 5-2) collected at the same location within 0.5 h to 1 h time intervals display varying measured noble gas concentrations. Although we do not have at the moment a definitive explanation for these varying concentrations, we have no reasons to believe that these result from a sampling artifact, at least for most samples. In particular, if this were to be the case, this would have rendered impossible the identification of any patterns in our samples.

4.2. Preliminary Estimate of Recharge Altitudes and Equilibration Temperatures

[15] Concentrations of atmospheric noble gases dissolved in water record various physical parameters (e.g.,

Table 2. Measured He, Ne, Ar, Kr and Xe Elemental Concentrations and He and Ar Isotope Ratios for All Samples[a]

Sample No.	He 10^{-8} cm^3 STP g^{-1}	Ne 10^{-7} cm^3 STP g^{-1}	Ar 10^{-4} cm^3 STP g^{-1}	Kr 10^{-8} cm^3 STP g^{-1}	Xe 10^{-9} cm^3 STP g^{-1}	R/R_a ($\pm1\sigma$)[b]	(^{38}Ar/^{36}Ar) ($\pm1\sigma$)	(^{40}Ar/^{36}Ar) ($\pm1\sigma$)
				Santa Cruz				
sz1-1	4.68	1.67	2.65	5.88	8.04	1.18 (0.03)	0.1858 (0.0028)	294.5 (1.75)
sz2-1	5.17	1.71	2.62	5.72	7.57	1.86 (0.05)	0.1879 (0.0021)	295.2 (0.86)
sz2-2	5.08	1.69	3.06	6.02	8.33	1.85 (0.06)	0.1877 (0.0049)	292.0 (1.04)
sz3-1	5.63	1.57	2.90	6.46	8.69	3.15 (0.08)	0.1835 (0.0033)	296.8 (0.96)
sz3-2	6.67	1.77	2.70	6.49	7.97	3.02 (0.09)	0.1882 (0.0024)	296.9 (0.96)
sz4-1	4.26	1.49	2.80	6.42	8.58	0.95 (0.04)	0.1920 (0.0044)	296.5 (1.36)
				San Cristobal				
sc1-1	4.49	1.65	3.21	6.80	9.13	1.02 (0.02)	0.1905 (0.0038)	293.8 (0.99)
sc1-2	4.53	1.63	3.38	6.89	9.52	1.03 (0.02)	0.1849 (0.0008)	291.8 (1.81)
sc2-1	3.93	1.49	2.60	5.76	8.12	1.01 (0.03)	0.1898 (0.0037)	295.6 (1.15)
sc2-2	4.60	1.61	3.13	6.86	9.53	0.97 (0.03)	0.1892 (0.0017)	296.2 (1.38)
sc3-1	4.38	1.59	2.81	6.09	8.37	0.97 (0.02)	0.1876 (0.0031)	294.8 (1.53)
sc3-2	4.42	1.55	2.83	4.93	6.35	0.99 (0.02)	0.1845 (0.0015)	291.1 (0.94)
sc4-1	4.45	1.63	2.62	5.49	7.30	1.04 (0.03)	0.1875 (0.0015)	293.8 (0.76)
sc4-2	4.22	1.53	2.90	6.30	8.27	1.01 (0.03)	0.1903 (0.0040)	295.5 (1.11)
sc5-1	5.18	1.72	2.87	5.57	7.40	0.96 (0.03)	0.1868 (0.0023)	294.4 (0.62)
sc5-2	4.72	1.58	2.78	5.56	7.65	1.13 (0.08)	0.1850 (0.0024)	293.4 (1.11)
sc6-1	4.47	1.51	2.62	5.46	7.29	1.05 (0.10)	0.1921 (0.0038)	292.6 (2.40)
sc6-2	3.84	1.48	2.20	4.50	6.17	1.02 (0.02)	0.1935 (0.0025)	296.1 (0.84)
sc8-1	4.52	1.67	2.86	5.69	7.46	0.99 (0.02)	0.1948 (0.0033)	294.5 (0.91)
sc9-1	4.92	1.81	2.97	5.99	8.27	0.98 (0.01)	0.1927 (0.0033)	294.5 (0.97)
sc9-2	5.03	1.86	2.87	5.89	8.24	0.98 (0.03)	0.1857 (0.0016)	295.6 (0.74)
sc10-1	4.25	1.66	3.05	6.38	8.41	0.98 (0.02)	0.1850 (0.0016)	295.5 (0.84)
sc10-2	4.68	1.62	2.99	6.34	8.89	1.16 (0.08)	0.1901 (0.0049)	293.5 (0.98)
sc11-1	4.60	1.74	2.80	5.82	7.87	1.00 (0.02)	0.1869 (0.0016)	296.8 (1.49)
sc11-2	4.82	1.67	2.96	7.04	8.66	1.09 (0.07)	0.1833 (0.0027)	294.2 (1.03)
sc12-1	4.47	1.45	3.11	7.06	9.55	1.00 (0.03)	0.1822 (0.0041)	297.0 (1.18)
sc12-2	4.59	1.74	3.01	6.32	8.51	1.01 (0.02)	0.1855 (0.0024)	296.5 (0.80)
sc13-1	4.57	1.66	2.85	5.98	8.09	1.01 (0.03)	0.1864 (0.0032)	295.0 (1.07)
sc13-2	4.48	1.67	3.07	5.72	7.61	1.00 (0.03)	0.1855 (0.0024)	293.3 (0.70)
ASW at 20°C, 0M NaCl, 0% excess air, 0 m altitude	4.48	1.85	3.12	6.98	9.57		0.1880	295.5
ASW at 20°C, 0 M NaCl, 0% excess air, 421 m altitude	4.26	1.76	2.96	6.63	9.09			

[a]Measurement errors of noble gas concentrations are ±1.5%, ±1.3%, ±1.3%, ±1.5%, ±2.2% for He, Ne, Ar, Kr and Xe, respectively.
[b]Helium isotope ratios, $R = {}^3He/{}^4He$, are normalized by the atmospheric value of $R_a = 1.384 \times 10^{-6}$.

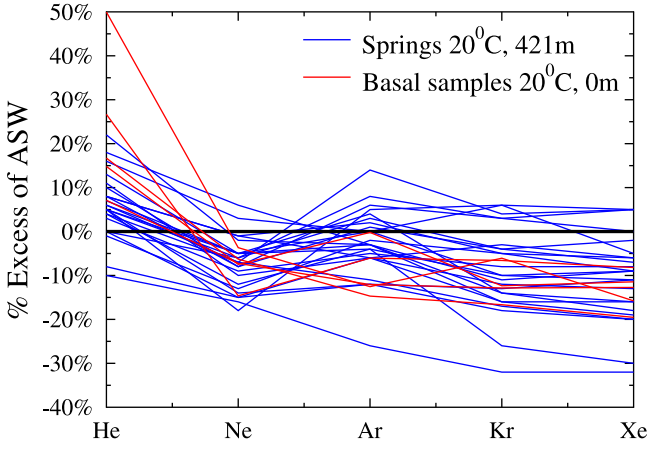

Figure 3. Measured noble gas concentrations relative to ASW at 20°C for all spring and basal aquifer samples from Santa Cruz and San Cristobal. Average altitude of 421 and 0 m asl. is assumed for all spring and basal aquifer samples, respectively. Noble gas concentrations with no addition or loss of dissolved gases as compared to ASW are indicated by a solid black line.

temperature, excess air, altitude, salinity) at which final equilibration takes place. While concentrations of all atmospheric noble gases dissolved in water decrease with temperature increase, their sensitivity to temperature increases with increasing atomic mass [*Mazor*, 1972]. Thus, while Xe concentrations are the most sensitive to temperature of equilibration, Ne concentrations are the least. Hence, Ne concentrations normalized to Xe concentrations (Ne/Xe) will be independent of recharge altitude and mostly sensitive to temperature of equilibration. On the other hand, 1/Xe will depend on both temperature and recharge altitude of equilibration. Indeed, an increase in recharge altitude proportionally decreases concentrations of all dissolved noble gases due to a decrease in partial pressures of noble gases in the atmosphere.

[16] Such a plot of 1/Xe versus Ne/Xe can be used to estimate an initial range of altitude and temperature of equilibration for all our Galapagos water samples by comparing measured Ne and Xe concentrations along with loci of calculated expected values for ASW (Figure 4). Such a simplified comparison with ASW does not account for the addition of the excess air (A) component resulting from dissolution of small air bubbles due to rapid water table fluctuations [*Heaton and Vogel*, 1981]. Because the presence of Ne in water is particularly indicative of the addition

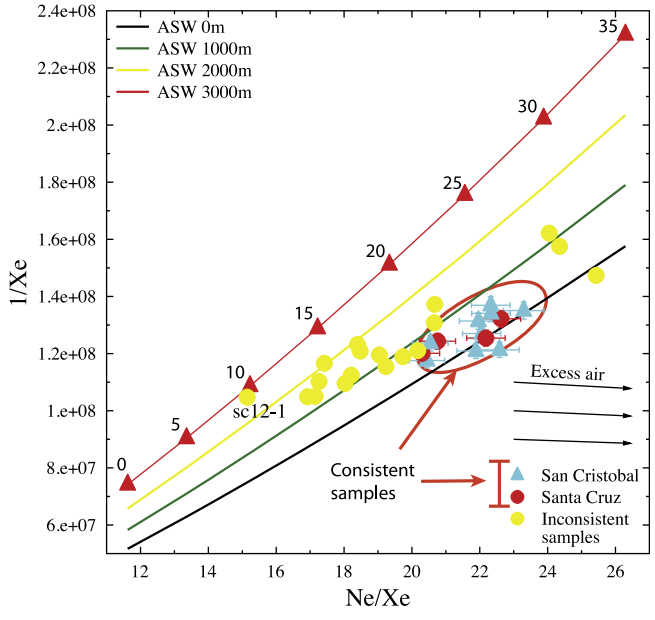

Figure 4. Preliminary estimate of recharge altitude and temperature by comparing measured 1/Xe versus Ne/Xe for all consistent and inconsistent San Cristobal and Santa Cruz samples with theoretical ASW values. Y axis is a function of temperature and pressure (altitude) and X axis depends only on temperature. Solid lines indicate ASW values at altitudes between 0–3000 m and solid markers indicate temperatures between 0–35°C. Addition of excess air moves samples in the direction indicated.

or loss of excess air [*Herzberg and Mazor*, 1979], any addition of excess air will move samples to the right hand side of the diagram as indicated in Figure 4, while any excess air loss will move samples in the opposite direction.

[17] Figure 4 shows all samples together with 1/Xe and Ne/Xe calculated for ASW at altitudes varying between 0 and 3000 m and temperatures varying between 0 and 35°C. With the exception of one sample from San Cristobal (Sc12–1), which points to a recharge altitude >2000 m and a temperature of 10°C, comparison between measured data and calculated ASW values suggests that recharge altitudes of all samples from both Santa Cruz and San Cristobal vary from 0 m to 2000 m for temperatures varying between ~15°C and ~30°C. It is thus apparent that many samples, more specifically 16 samples, are recording equilibration recharge altitudes and temperature conditions that are not consistent with conditions on the ground. In sections 5, 6, and 7, these 16 samples are referred to as "inconsistent". In particular, some of these recharge altitudes are far greater than the summits of both Santa Cruz (870 m) and San Cristobal (730 m), and some of the temperatures are too low to be observed within the islands during either the "garúa" or the hot season. The unexpected observed relative Ar excess as well as depletion of Ne, Kr and Xe in inconsistent Galapagos samples points to unique equilibration processes that do not conform to key assumptions of the noble gas thermometer and NGT calculations [e.g., *Ballentine and Hall*, 1999; *Aeschbach-Hertig et al.*, 2000]. These mechanisms and, in particular, samples that display these unexpected noble gas patterns, are discussed later in this manuscript (cf. section 7). Below we discuss results for all noble gas samples that display recharge altitudes and temperatures consistent with those in place in the islands, and show how NGTs and stable isotopes can be used to provide constraints both on recharge location and timing of recharge. These samples are referred to as "consistent" samples. Both consistent and inconsistent samples are clearly indicated in Figure 4. In addition, by using R/Ra ratios for all spring samples together with tritium measurements in precipitation, we place constraints on groundwater residence times for the perched aquifers of both islands (cf. section 6).

5. Constraining Recharge Areas and Timing of Recharge

5.1. Noble Gas Temperatures

[18] Noble gas temperatures (NGTs) derived from groundwater are generally assumed to reflect the mean annual air temperature (MAAT) and pressure conditions at the base of the aerated zone [*Stute and Sonntag*, 1992]. While this assumption has been verified through field experiments in sedimentary systems [*Klump et al.*, 2007], this might not be the case in mountain groundwater flow systems [*Manning and Solomon*, 2003]. Because of the presence of preferential flow paths in basaltic systems (e.g., fractures, lava tunnels), it is plausible that recharge water in these systems might reflect the temperature of the ground surface at the precise time of infiltration rather than the mean annual air temperature value as commonly assumed in sedimentary systems. Temperatures and altitudes at the time of recharge can be inferred using a standard unfractionated air (UA) model [*Stute and Schlosser*, 1993]. While the UA model provides an unbiased estimate of recharge altitude, the closed system equilibration (CE) model [*Aeschbach-Hertig et al.*, 2008] estimates recharge altitudes that are biased to high values [see e.g., *Sun et al.*, 2010].

[19] The UA model is the simplest lumped-parameter noble gas model that quantitatively accounts for both ASW and the presence of excess air in groundwater. Excess air is compositionally similar to atmospheric air [*Klump et al.*, 2007] and is lumped into a single parameter (A), representing the total volume of excess air per volume of water. Since the UA model assumes complete dissolution of excess air, final dissolved concentrations ($C_{i,final}$) for each noble gas i in water are given by the sum of air saturated water ($C_{i,eq}$) and excess air (A) as follows:

$$C_{i,final} = C_{i,eq}(1 + AH_i), \quad (1)$$

where H_i represents the Henry's constant for noble gas i. Measured final dissolved concentrations of all four noble gases (Ne, Ar, Kr and Xe) are inverted for NGTs and constrained excess air ($A \geq 0$) assuming a particular recharge altitude value [cf., *Ballentine and Hall*, 1999]. While inverse problems that simultaneously estimate NGTs, excess air and recharge altitude using only measured Ne, Ar, Kr and Xe are ill posed, unique values for NGTs and excess air are obtained if recharge altitudes are known [*Manning and Solomon*, 2003].

[20] UA model NGTs were calculated for all consistent water samples assuming various recharge altitudes, varying

from sampling/spring altitude, which represents the minimal possible recharge altitude, up to 1000 m (Figures 5a and 5b) for successive 50 m increments (cf. auxiliary material).[1] Because a nonnegative constraint is imposed on excess air, NGTs were derived only from those recharge altitudes that yielded zero or positive excess air values. Hence, a minimum recharge altitude for each sample was derived as the sampling altitude with nonnegative excess air or lowest altitude beyond the sampling altitude with zero excess air. Figure 5 shows the results of all consistent samples calculated NGTs for individual water samples as a function of altitude compared with all possible altitude and temperature values within both islands. NGTs for individual water samples were first compared with extreme temperature-altitude relationships in Santa Cruz (Figure 5a) and San Cristobal (Figure 5b) as described in Appendix A.

[21] Comparison between calculated sample NGTs and corresponding altitudes with extreme temperature-altitude transects in these islands clearly show that four Santa Cruz samples (sz1-1, 2-1, 2-2, 3-2) and nine San Cristobal samples (sc4-1, 5-1, 8-1, 9-1, 9-2, 11-1, 12-2, 13-1, 13-2) point to recharge occurring at temperatures and altitudes which are consistent with those in place in the islands (Figures 5a and 5b). Overall, it is apparent that recharge altitudes between 160 and 870 m and temperatures between 20.05 ± 2.07°C and 27.54 ± 0.47°C are found for Santa Cruz basal aquifer samples (Figure 5a) while recharge altitudes between 229 and 730 m and temperatures of 19.95 ± 1.13°C and 26.36 ± 0.66°C are found for San Cristobal spring samples (Figure 5b), suggesting that these are the altitude and temperature range values at which recharge occurs in these two islands, respectively. In addition, the minimum possible recharge altitude for four San Cristobal samples (Sc5-1, 9-1, 9-2, 11-1) and one Santa Cruz sample (Sz3-2) are the same as their sampling altitudes suggesting that some local recharge water may also contribute to these springs and basal aquifer. Maximum possible recharge altitudes for 12 out of 13 consistent samples from both San Cristobal and Santa Cruz correspond to the peak altitude of the islands as shown in Figure 5. However, sz2-1 points to a maximum recharge altitude of 750 m as corresponding NGTs beyond 750 m are greater than the extreme maximum temperature transect (cf. Figure 5a).

[22] NGTs for consistent individual water samples are also compared with average seasonal temperatures in Santa Cruz and San Cristobal to constrain timing of recharge. Shaded regions indicate average seasonal temperatures $\pm 1\sigma$ (Figure 5, dark green and pink for "garúa" and hot season, respectively, light green, transition between the two). Average seasonal temperature versus altitude in Santa Cruz was derived by extrapolating the average (1964–2010) "garúa" (22.63 ± 3.39°C) and hot season (25.9 ± 1.98°C) temperatures in Puerto Ayora, by assuming a temperature gradient of −0.8°C/100 m. Average seasonal temperature versus altitude in San Cristobal was derived by extrapolating the average (1985–2005) "garúa" (23.57 ± 3.38°C) and hot season (26.53 ± 2.72°C) temperature in Puerto Bacquerizo Moreno (7.9 m asl), assuming a temperature gradient similar to that of Santa Cruz.

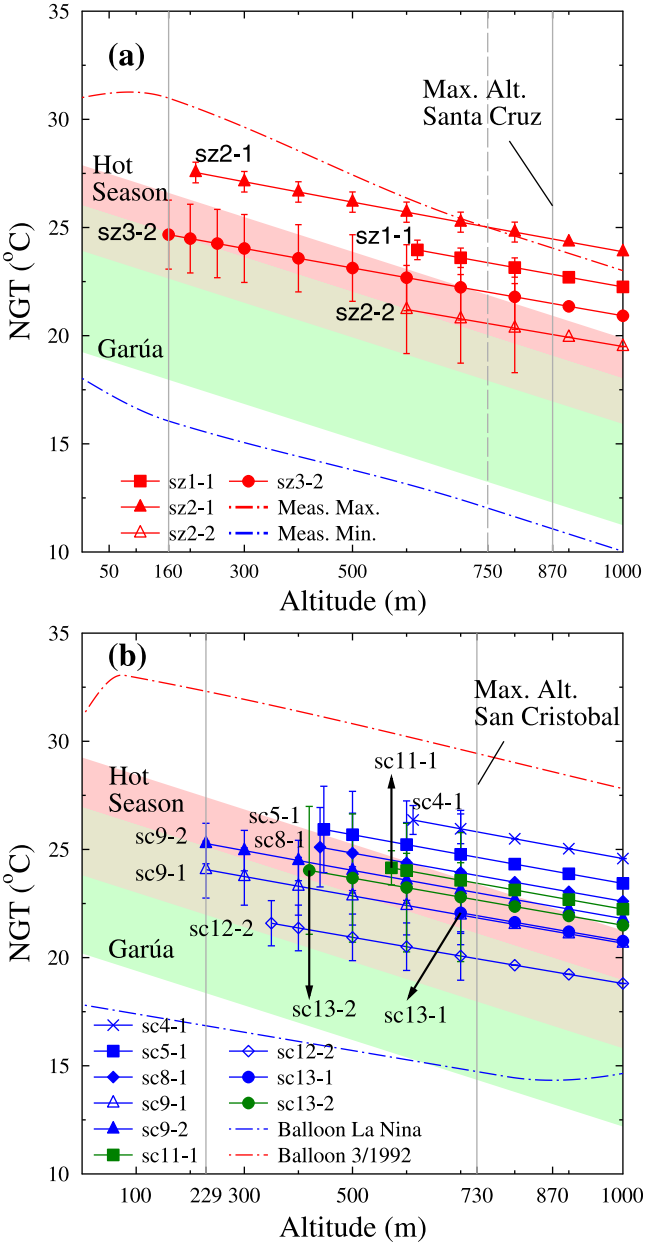

Figure 5. NGTs calculated assuming recharge altitudes for samples that fall within expected temperature and altitude ranges (a) Santa Cruz NGTs compared with monthly mean maximum and minimum temperatures during (3/1992) and (9/2007) at Puerto Ayora and Bellavista. Shaded regions are average (1965 to 2010) "garúa" and hot season tem- peratures at Puerto Ayora ±1 σ. Maximum, minimum and shaded average seasonal temperatures extrapolated using average gradient of −0.8°C/100 m. (b) San Cristobal NGTs compared with monthly mean measured weather balloon temperatures during La Nina (9/2007) for extreme minimum and El Nino (3/1992) plus mean diurnal variation (7.15°C) for extreme maximum temperatures. Shaded regions indicate average (1985 to 2005) "garúa" and hot season temperatures at Puerto Baquerizo Moreno ±1 σ, extrapolated using a gradient of −0.8°C/100 m.

[1]Auxiliary materials are available in the HTML. doi:10.1029/2011WR010954.

[23] Our NGT comparison for consistent water samples in Santa Cruz with the derived average seasonal temperature (Figure 5a) points unequivocally to dominant recharge during the hot season. All these samples are located in the basal aquifer. In addition, with the exception of one spring sample (Sc12-2), all other spring samples in San Cristobal (which display expected altitude and temperatures) point also to recharge occurring predominantly during the hot season (Figure 5b). It is of relevance to note that all these spring samples are located at low altitudes (<∼420 m asl). Based on these results, we can thus conclude that low-altitude perched aquifers are also dominantly recharged during the hot season. Sc12-2, on the other hand, indicates likely recharge during both the "garúa" and the hot season.

[24] As shown above, noble gases can be used as an effective tool to identify recharge areas as well as timing of recharge in fractured areas in general and basaltic aquifer systems in particular. Our NGT comparison for consistent water samples with expected altitude and temperature patterns points to recharge of all our basal aquifer samples in Santa Cruz and all low-altitude springs (except sc12-2) in San Cristobal predominantly during the hot season. As seen below, NGT derived results on timing of recharge are corroborated by stable isotope analyses obtained for these same samples.

5.2. Stable Isotopes

[25] Stable isotope analyses of all Santa Cruz samples yield δD and $\delta^{18}O$ values between −13.5‰ and −8.85‰, and −3.1‰ and −2.13‰, respectively (Table 3, Figure 6a). Springs in San Cristobal yield δD and $\delta^{18}O$ between −11.46‰ and −5.96‰, and −2.74‰ and −1.95‰, respectively (Table 3, Figure 6a). While most samples lie either on the Global Meteoric Water line (GMWL) [*Craig*, 1961] or show deuterium excess [*Dansgaard*, 1964], Santa Cruz basal aquifer sample sz1 and San Cristobal El Junco lake sample sc3 in particular, lie to the far right of GMWL (Figure 6a) and display significant $\delta^{18}O$ excess (∼0.5‰ and ∼3‰, respectively) assuming an evaporation slope of

Table 3. Measured Stable Isotope Composition of Water Samples Along With Sample Numbers

Sample No.	^{18}O (‰)	±1σ	δD (‰)	±1σ
		Santa Cruz		
sz1	−2.13	0.06	−8.85	0.52
sz2	−2.55	0.09	−10.06	0.41
sz3	−2.60	0.06	−10.57	0.67
sz4	−3.10	0.06	−13.50	1.03
		San Cristobal		
sc1	−2.31	0.08	−7.13	0.62
sc2	−2.10	0.07	−6.81	0.71
sc3	0.89	0.07	6.54	0.69
sc4	−2.74	0.08	−11.46	0.52
sc5	−2.07	0.06	−6.04	0.71
sc6	−1.95	0.06	−6.40	0.73
sc8	−2.69	0.07	−8.71	0.90
sc9	−2.63	0.09	−8.76	0.50
sc10	−2.22	0.06	−5.96	0.96
sc11	−2.38	0.06	−7.72	0.88
sc12	−2.30	0.07	−7.91	1.04
sc13	−2.60	0.06	−9.70	0.90

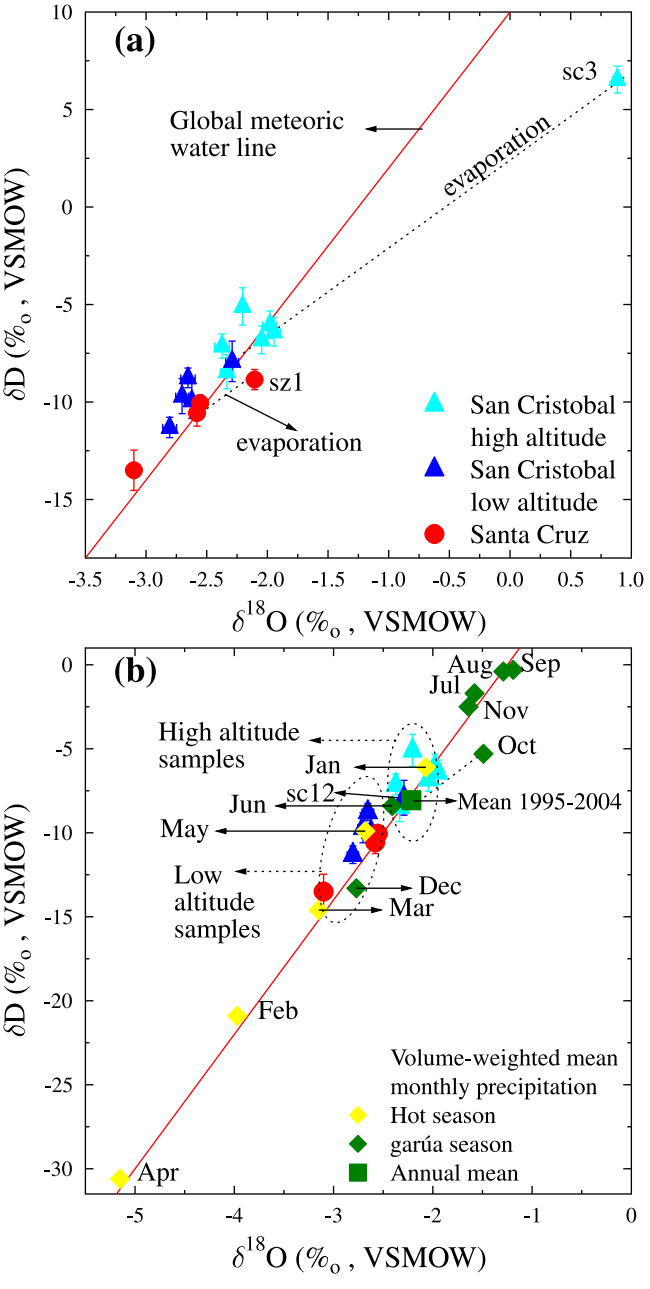

Figure 6. (a) Measured δD and $\delta^{18}O$ values of all water samples from San Cristobal (triangles) and Santa Cruz (circles) compared with the global meteoric water line [*Craig*, 1961]. Samples with possible evaporation effects are indicated by dashed lines. $\delta^{18}O$ excess values are calculated assuming an evaporation slope of 4.5. (b) Stable isotope ratios of all water samples compared with volume-weighted mean (1995–2004) monthly values for rainfall at Bellavista (diamonds). Mean monthly values from hot season (yellow diamonds) are less enriched than those from the "garúa" season (green diamonds). Ellipses indicate high- and low-altitude sample clusters. High-altitude (>∼420 m) samples are more enriched than low-altitude samples and are indicated.

4.5. Such $\delta^{18}O$ excess is likely the result of kinetic fractionation during evaporation [*Dansgaard*, 1964]. As a result, both sz1 and lake El Junco are thus excluded from the discussion below. In the discussion that follows, all other water samples from both San Cristobal and Santa Cruz are compared with volume-weighted monthly mean rainfall isotopic composition in order to constrain timing of recharge.

[26] Volume-weighted mean monthly values of stable isotopic composition in rainfall were obtained from the closest available isotope monitoring station (International Atomic Energy Agency/World Meteorological Organization, Global Network of Isotopes in Precipitation., The GNIP Database, available at http://www.iaea.org/water, 2006), located in Bellavista, Santa Cruz, at an elevation of 194 m between 1995 and 2004 (Figure 6b, diamonds). Because peak altitudes of both islands are not very high and the progress of the trade-wind generated rainout process of atmospheric vapor, which induces the altitude effect, is halted at the base of the stable inversion layer at an elevation of ~300 m, mean monthly rainfall isotopic composition during the "garúa" season was not corrected for the altitude effect [*Gonfiantini et al.*, 2001]. With the exception of October, all other mean monthly isotopic composition (Figure 6b) lie next to the global meteoric water line (GMWL) [*Craig*, 1961]. Mean monthly October isotopic composition deviates to the right of the GMWL, and displays an excess in $\delta^{18}O$ of 0.94‰ which might be an indication of lower-humidity conditions generally observed during this month [*Dansgaard*, 1964; *Gonfiantini et al.*, 2001].

[27] Except for the mean monthly isotopic concentrations of transition months between both seasons, January and December, between the "garúa" and the hot season, and June, transition from hot to the "garúa" season, all other mean monthly rainfall values for both the "garúa" (July–November) and the hot season (February–May) display very distinct, marked signatures as compared to the annual mean value of precipitation (Figure 6b). While December and June show significant depletion in stable isotopic composition compared to precipitation during the "garúa" season, January shows significant enrichment compared to storm rain samples from the hot season. Excluding the transition months, precipitation during the hot season is more depleted than the annual mean value of precipitation while precipitation during the "garúa" season is more enriched than the annual mean value of precipitation (Figure 6b). Similar isotope observations of precipitation during the hot season compared to the dry season have been reported in a number of tropical regions [*Scholl et al.*, 1996; *Gonfiantini et al.*, 2001; *Scholl et al.*, 2002] and have been attributed to the amount effect [*Dansgaard*, 1964]. This distinct seasonality in isotopic composition of rainfall between the "garúa" and the hot season months as compared to the annual mean is used to identify the timing of recharge for all water samples.

[28] All our water samples fall well within the monthly average rainfall isotopic end members, April ($\delta D = -5.15$‰, $\delta^{18}O = -30.6$‰) for the hot season, and September ($\delta D = -1.19$‰, $\delta^{18}O = -0.3$‰) for the "garúa" season (Figure 6b). Specifically, Santa Cruz samples (sz2, 3, 4) fall within the domain of depleted precipitation during the hot season indicating likely recharge during this season. These stable isotope comparisons reaffirm our NGT results for basal aquifer samples from Santa Cruz that recharge occurs predominantly during the hot season. Similarly, four spring samples from San Cristobal (sc4, 8, 9, 13) also lie closer to the more depleted rain water samples from intense precipitation events during the hot season. Of relevance is the fact that all these spring samples which lie closer to the hot season isotopic signature, belong to the same subset of low-altitude spring samples observed using NGTs (Figure 6b). Similar to observations based on NGTs, isotopic compositions of low-altitude spring samples also indicate that recharge might predominantly occur during the hot season. In contrast, seven (sc1, 2, 5, 6, 10, 11, 12) spring samples (Table 3) are more enriched than rain water samples from the hot season. These spring samples lie between the subset of enriched "garúa" rainfall samples and the depleted hot season rainfall samples indicating that recharge during both seasons might potentially be important for these springs. More importantly, all seven of these enriched samples (except sc12) are also located at high altitudes (>~420 m).

[29] Results obtained using NGTs and stable isotope analyses thus lead to a common conclusion, i.e., samples predominantly recharged during the hot season are found at lower altitudes (<~420 m asl), while samples pointing to recharge during both seasons appear to be located at higher altitudes (>420 m asl). This suggests that the composition of recharge water at different altitudes follows the distribution of rainfall rather closely as shown in Figure 2b. These results are in agreement with previous findings based on the distribution of effective rainfall (Figure 2b) [*d'Ozouville et al.*, 2008a], which show that precipitation during the "garúa" season is more prevalent at higher altitudes (cf. section 2).

[30] It is interesting to note that the high-altitude samples, which point to recharge during both seasons using stable isotopes are precisely those displaying inconsistent recharge altitudes and temperatures using noble gases. In section 7, we explore various mechanisms to explain the unexpected relative Ar enrichment and Ne, Kr and Xe depletion observed in 16 inconsistent samples out of a total of 29 water samples, which lead to inconsistent recharge altitudes and temperatures using standard NGT models. Below, through measured He isotopic ratios in springs together with tritium measurements in precipitation we place constrains in the groundwater residence times. These are fairly young and further reinforce the notion that NGTs do indeed record seasonality in fractured systems rather than the MAAT commonly assumed in sedimentary systems. *Thoma et al.* [2011] have recently come to a similar conclusion.

6. Tritium/^{3}He Groundwater Residence Times

[31] Our combined NGTs and stable isotope analyses independently record seasonal climatic signals for all samples from San Cristobal and Santa Cruz. Among other factors, preservation of seasonal climatic signals is dependent on the presence of a shallow water table and short groundwater residence times [e.g., *Stute and Schlosser*, 1993; *Thoma et al.*, 2011]. Below, we provide a first-order estimate of groundwater residence times for all spring samples based on the presence of marginal He excesses in springs (cf. section 4.1) derived from β decay of natural

and bomb ^{3}H and verify that all springs indeed display young groundwater ages. Estimation of groundwater residence times for the basal aquifer samples based on tritiogenic He are not possible due to a significant presence of mantle He which complicates the tritiogenic versus mantle ^{3}He separation (cf. section 4.1) [see also *Schlosser*, 1989].

[32] Tritiogenic ^{3}He concentrations for each spring are calculated from measured R/R_a ratios (Table 2) and measured ^{4}He concentrations (^4He_m, Table 4) following *Schlosser et al.* [1988], assuming ^{4}He concentrations in equilibrium with the atmosphere (ASW). ^{4}He concentrations in equilibrium with the atmosphere corresponding to a wide range of possible temperatures and altitudes on both islands were used to estimate tritiogenic ^{3}He concentrations and subsequently tritium ages in each spring sample (cf. auxiliary material). Because tritiogenic ^{3}He concentrations and derived tritium ages for all spring samples are insensitive to the chosen equilibrium conditions (cf. auxiliary material), below, we discuss only results obtained by assuming ^{4}He equilibrium at maximum possible altitudes and their corresponding MAATs.

[33] Table 4 shows the results of calculated tritiogenic ^{3}He in tritium units (TU; 1 TU = 2.5×10^{-15} cm^3 STP g^{-1} ^{3}He) for each spring sample along with its error ($\pm 1\sigma$). Tritiogenic ^{3}He errors were calculated using a propagation of errors from estimated analytical error estimates. Results show that, within error, the amount of tritiogenic ^{3}He (in TU) required to account for the marginal ^{3}He excesses observed in many spring samples (cf. section 4.1) varies between ~0 TU and 4.45 ± 2.13 TU (Table 4). The calculated amount of ^{3}He excess for each spring sample is then compared with available historical records of ^{3}H in local precipitation. ^{3}H in precipitation was measured continuously between 1995 and 2007 at Bellavista, Santa Cruz (Figure 7; International Atomic Energy Agency/World Meteorological Organization, online, 2006). The ^{3}H record for precipitation at Bellavista shows a background ^{3}H of 1.02 TU with two ^{3}H peaks corresponding to 7.66 ± 0.41 TU in 10/1999, which only lasted for a month, and a subsequent peak in 02/2004 with a maximum of 14.55 ± 1.4 TU, which lasted the entire year, yielding an annual average ^{3}H value in 2004 of 10.11 ± 3.07 TU. Excess ^{3}He added to the groundwater by the decay of each of the above three ^{3}H maximum values (7.66 ± 0.41 TU, 14.55 ± 1.4 TU and 10.11 ± 3.07 TU) until the sampling date (October, 2007) can be estimated based on its half-life of 12.43 years (Figure 8a). It should be noted that the amount of ^{3}He available from the decay between 10/1999 and 10/2007 (green line, Figure 8a) would yield the highest ^{3}He availability because of the combined addition of ^{3}He from the decay of ^{3}H maximum in 10/1999 and 2004. Comparison of the amount of estimated tritiogenic ^{3}He (blue triangles, Figure 8a) with the amount of tritiogenic ^{3}He available from decay of ^{3}H in precipitation (green, red and blue lines, Figure 8a) shows that within errors, both the amount of tritiogenic ^{3}He available in 10/2007 from decay of ^{3}H between 10/1999 and 10/2007 (green line, Figure 8) as well as between 02/2004 and 10/2007 (red line, Figure 8a) are sufficient to account for the estimated tritiogenic ^{3}He for all spring samples. It is relevant to note that decay of ^{3}H between the 2004 annual average of 10.11 ± 3.07 TU and 10/2007 can account for the tritiogenic ^{3}He for all samples except sc5-2 and sc10-l and

Table 4. Tritiogenic ^{3}He Required for He Excesses in All Springs Along With ^{3}H/^{3}He Ages for Different Assumed ^{3}H Maximums

Sample	^4He_m 10^{-8} cm^3 STP g^{-1}	$\pm 1\sigma$ 10^{-10} cm^3 STP g^{-1}	^{3}He/^{4}He $\times 10^{-6}$	$\pm 1\sigma \times 10^{-6}$	$^3He_{required}$ ($\pm 1\sigma$) (TU)	^{3}H/^{3}He Ages: 02/2004 (Years ± 1σ)[a]	^{3}H/^{3}He Ages: mean 2004 (Years ± 1σ)[b]	^{3}H/^{3}He Ages: 10/1999 (Years ± 1σ)[c]
sc1-l	4.49	6.74	1.409	0.032	0.84 (0.57)	1.21 (0.81)	1.69 (1.14)	2.66 (1.82)
sc1-2	4.53	6.79	1.430	0.033	1.22 (0.61)	1.74 (0.84)	2.41 (1.18)	3.75 (1.90)
sc2-1	3.93	5.89	1.398	0.044	0.61 (0.70)	0.89 (1.00)	1.24 (1.39)	1.96 (2.20)
sc2-2	4.60	6.90	1.338	0.039	−0.46 (0.72)	−0.69 (1.12)	−0.99 (1.61)	−1.63 (2.72)
sc3-1	4.38	6.57	1.348	0.030	−0.24 (0.54)	−0.37 (0.82)	−0.52 (1.17)	−0.86 (1.94)
sc3-2	4.42	6.63	1.363	0.029	0.02 (0.52)	0.03 (0.77)	0.04 (1.09)	0.07 (1.76)
sc4-2	4.22	6.34	1.402	0.037	0.69 (0.63)	1.01 (0.90)	1.41 (1.26)	2.23 (2.00)
sc5-2	4.72	7.08	1.563	0.104	3.78 (1.97)	4.91 (2.30)	–	9.72 (4.40)
sc6-1	4.47	6.71	1.453	0.137	1.63 (2.46)	2.29 (3.25)	3.16 (4.39)	4.86 (6.52)
sc6-2	3.84	5.75	1.406	0.032	0.73 (0.49)	1.06 (0.70)	1.48 (0.98)	2.34 (1.58)
sc10-l	4.25	6.38	1.349	0.025	−0.20 (0.43)	−0.31 (0.65)	–	−0.71 (1.53)
sc10-2	4.68	7.01	1.600	0.113	4.45 (2.13)	5.66 (2.40)	7.55 (3.13)	11.01 (4.52)
sc11-2	4.82	7.24	1.506	0.096	2.75 (1.85)	3.70 (2.29)	5.03 (3.04)	7.56 (4.47)
sc12-l	4.47	6.71	1.390	0.035	0.49 (0.62)	0.72 (0.90)	1.00 (1.25)	1.60 (1.99)
sc4-l	4.45	6.67	1.442	0.036	1.43 (0.64)	2.02 (0.89)	2.79 (1.24)	4.32 (2.01)
sc5-l	5.18	7.76	1.323	0.044	−0.88 (0.92)	−1.36 (1.50)	−1.96 (2.20)	−3.28 (3.90)
sc8-l	4.52	6.78	1.372	0.033	0.16 (0.60)	0.24 (0.89)	0.34 (1.25)	0.55 (2.01)
sc9-l	4.92	7.38	1.356	0.018	−0.16 (0.36)	−0.24 (0.54)	−0.34 (0.77)	−0.55 (1.26)
sc9-2	5.03	7.55	1.349	0.042	−0.31 (0.84)	−0.47 (1.29)	−0.67 (1.85)	−1.09 (3.07)
sc11-l	4.60	6.91	1.381	0.030	0.34 (0.56)	0.50 (0.82)	0.70 (1.15)	1.12 (1.83)
sc12-2	4.59	6.89	1.398	0.030	0.64 (0.56)	0.94 (0.80)	1.31 (1.12)	2.08 (1.79)
sc13-l	4.57	6.85	1.402	0.040	0.72 (0.74)	1.04 (1.05)	1.46 (1.45)	2.30 (2.29)
sc13-2	4.48	6.72	1.384	0.044	0.39 (0.80)	0.57 (1.16)	0.80 (1.62)	1.28 (2.56)
sz4-l	4.26	6.39	1.320	0.050	−0.71 (0.85)	−1.09 (1.36)	−1.56 (1.98)	−2.59 (3.45)

[a] ^{3}H/^{3}He age calculated assuming ^{3}H peak of 14.55 ± 1.4 TU in 02/2004.
[b] ^{3}H/^{3}He age calculated assuming mean of ^{3}H peak in 2004 of 10.11 ± 3.07 TU.
[c] ^{3}H/^{3}He age calculated assuming ^{3}H peak of 7.66 ± 0.41 TU in 10/1999.

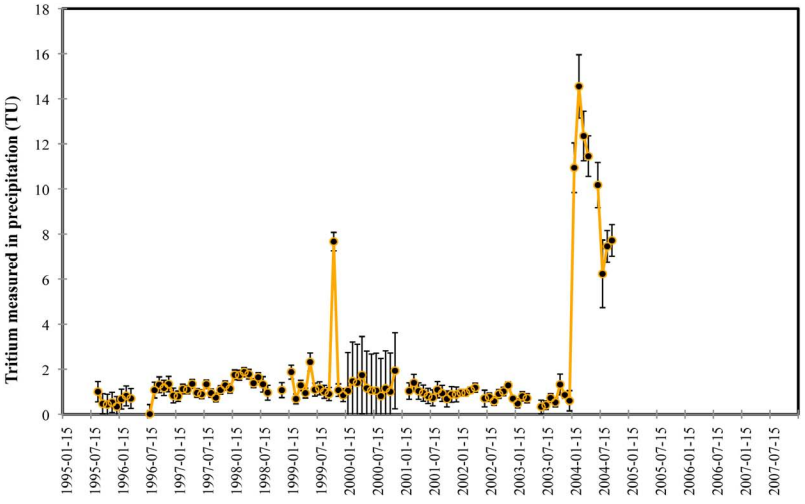

Figure 7. Historical record of tritium measurements in precipitation (International Atomic Energy Agency/World Meteorological Organization, online, 2006) between 1995 and 2007 at Bellavista, Santa Cruz. Background tritium measurement of 1.02 TU along with two identifiable ^{3}H peaks corresponding to 7.66 ± 0.41 TU in 10/1999, which only lasted for a month, and a subsequent peak in 02/2004 with a maximum of 14.55 ± 1.4 TU, which lasted the entire year is observed. Tritium measurements in 2004 yield an annual average of 10.11 ± 3.07 TU.

tritium ages are not estimated for those samples. Apparent tritium ages were calculated following:

$$t = \frac{12.43}{\ln 2} \times \ln\left(1 + \frac{[^3\mathrm{He}]}{[^3\mathrm{H}]}\right), \qquad (2)$$

where, t is tritium age in years, [^{3}He] is the calculated amount of tritiogenic ^{3}He in spring samples and [^{3}H] is the measured tritium concentration of groundwater. Although no tritium measurements are available for our groundwater samples, as a first-order approximation, it is assumed that present tritium concentrations in our spring samples result from the decay of one of the above ^{3}H maximums. Such an assumption is expected to yield an upper limit to tritium ages for all springs because the presence of additional tritium from previous unrecorded maximums, if any, would yield younger ages according to equation (2). Because the calculation of

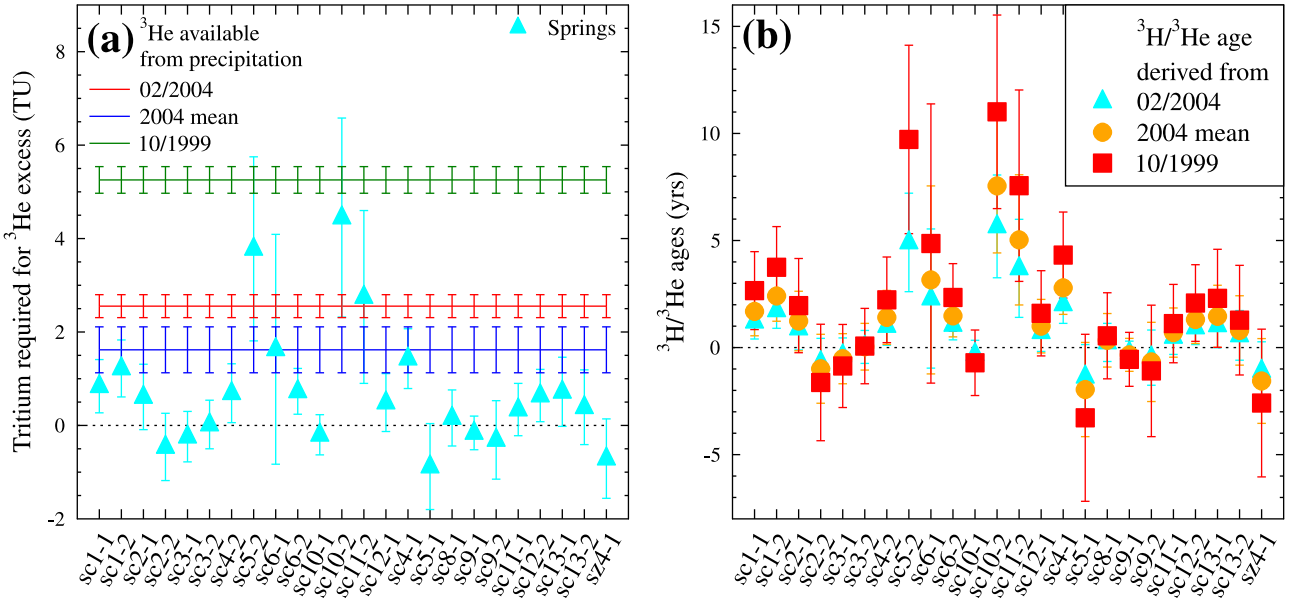

Figure 8. Tritium/^{3}He analysis of all springs from San Cristobal and Santa Cruz (a) Comparison of ^{3}He excess for all springs with ^{3}He available from precipitation assuming decay of ^{3}H peaks on 10/1999, 02/2004 and mean 2004 (b) Tritium/^{3}He ages derived from ^{3}He excess for each spring and assuming tritium concentration in groundwater resulting from the decay of ^{3}H maximums on 10/1999, 02/2004 and mean 2004.

tritium ages is based on the assumption that ^{3}H maximums can account for the measured amount of tritiogenic ^{3}He in all samples, tritium ages were not calculated for samples sc5-2 and sc10-1 using the annual average maximum ^{3}H peak in 2004 (Table 4). For all other springs, tritium ages were calculated assuming a tritium concentration in groundwater that results from the decay of each of the three ^{3}H maximums, thus yielding a range of tritium ages for each sample.

[34] Table 4 shows tritium ages calculated for all spring samples assuming ^{3}H maximums in 10/1999, 02/2004 as well as the 2004 ^{3}H annual average. Our results show that maximum tritium ages are obtained for all spring samples assuming the 10/1999 ^{3}H maximum while minimum tritium ages are obtained for all spring samples assuming the 02/2004 ^{3}H maximum (Figure 8b). However, irrespective of assumed ^{3}H maximums, all springs yield groundwater ages that are very young. Within error, tritium ages for all springs vary between ~0 and 11 ± 4.5 years with a mean age of 2.03 years (corresponding to the 10/1999 maximum). In particular, all consistent spring samples correspond to a mean age 0.75 ± 7.25 years (corresponding to 10/1999 maximum) while the remaining inconsistent springs correspond to a mean age of 2.8 ± 12.4 years. However, poor age uncertainties associated with all spring samples presently do not allow for a definitive age resolution between consistent and inconsistent springs.

[35] Although derived tritium ages for all springs represents a first-order approximation, it is apparent that all spring samples, irrespective of assumption and measured tritium values used, are very young with short groundwater residence times. Short groundwater residence times associated with these springs corroborates results from NGTs and stable isotopes, which independently suggest preservation of seasonal climatic signals. As discussed earlier, high-altitude samples display unique noble gas patterns (cf. section 4.1) and yield inconsistent recharge altitudes and temperatures using noble gases (cf. section 4.2), while simultaneously pointing to recharge during both the "garúa" and hot season using stable isotopes (cf. section 5.2). Below, we explore various mechanisms to explain the unexpected noble gas patterns, particularly, relative Ar enrichment and Ne, Kr and Xe depletion observed in all inconsistent samples.

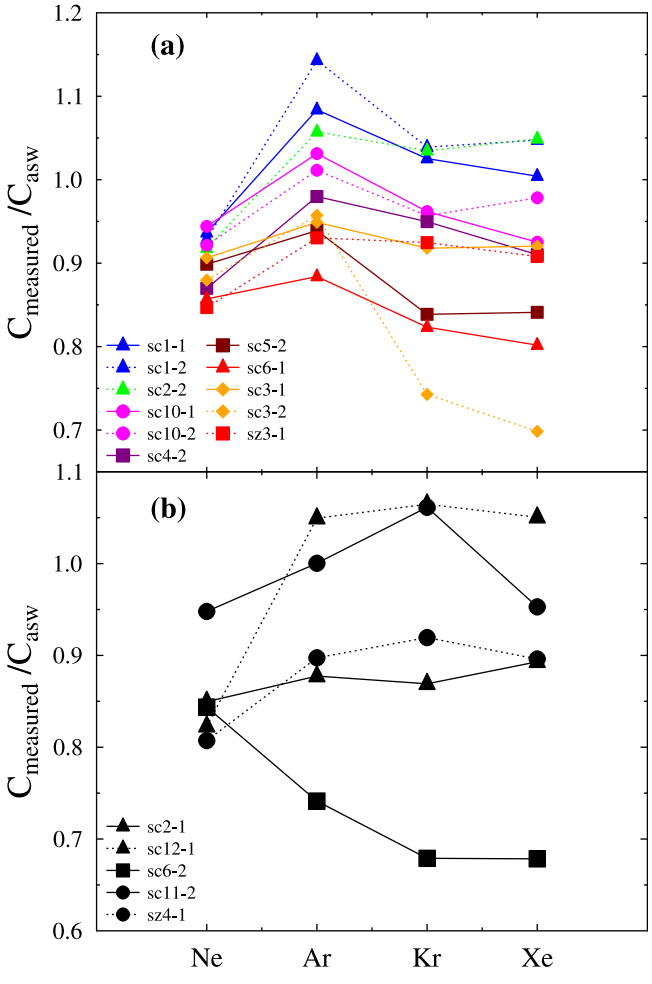

Figure 9. Measured Ne, Ar, Kr and Xe patterns for 16 inconsistent water samples normalized to air saturated water (ASW) at sea level and 421 m for all basal aquifer and spring samples, respectively. All samples were also normalized to average temperature of 20°C (a) Samples with a unique excess of nonradiogenic Ar relative to the concentrations of Ne, Kr and Xe. (b) Samples with systematic depletion (triangle) and excess (square) of lighter noble gases as compared to the heavier noble gases. Samples with a Kr "bump" are also shown (circles).

7. Potential Gas Loss Mechanisms in Fractured Environments

[36] Samples that display inconsistent recharge altitudes and temperatures with respect to those in place in Santa Cruz and San Cristobal using standard noble gas models [e.g., *Stute and Schlosser*, 1993; *Ballentine and Hall*, 1999; *Aeschbach-Hertig et al.*, 1999] also show systematic deviations of dissolved noble gases from expected ASW values. Figures 9a and 9b show the observed noble gas patterns for all 16 inconsistent samples normalized to ASW at average sampling elevations and temperatures in place in both islands (cf., section 4.1). For 11 out of the 16 samples, a common pattern emerges in which Ar excess relative to all other gases is observed (Figure 9a). The remaining five samples display varying signatures without similar trends (Figure 9b). In particular, sample sc6-2 (Figure 9b) shows an excess of the lighter noble gases Ne and Ar relative to the heavier noble gases Kr and Xe, a pattern similar to that predicted by standard noble gas models that account for the addition of excess air [*Aeschbach-Hertig et al.*, 2008]. By contrast, all other four samples show a pronounced loss of Ne over all other noble gases. In addition, samples sc11-2, sc12-1 and sz4-1 display also an excess of Kr relative to all other gases.

[37] Below we explore various mechanisms to assess their potential at reproducing the observed noble gas patterns, and, in particular, the observed relative Ar excess. Specifically, we test the extent of noble gas loss through existing degassing models, in addition to assessing the potential impact of fog droplets ("garúa" dew) on dissolved noble gas concentrations in groundwater and the effect of mixing between noble gas depleted rainwater

formed in the atmosphere at high-altitude ($\geq$1500 m) and low-altitude (>400 m) fog droplets. Such degassing models have never been tested in fractured, basaltic environments and the effect of mixing high-altitude rainwater with low-altitude fog droplets is an entirely untested process.

7.1. Modeling Loss of Dissolved Noble Gases Through Existing Degassing Models

[38] Groundwater degassing by partitioning of dissolved noble gases into an initially noble gas-free bubble has recently been observed in a number of environments including an ultra deep mine [*Lippmann et al.*, 2003], a hydrocarbon contaminated site [*Amos et al.*, 2005] and agricultural areas [*Visser et al.*, 2007; *Cey et al.*, 2008]. Existing degassing models describe the partitioning mechanisms involved in loss of dissolved noble gases as either a solubility equilibrium process (e.g., closed equilibration (CE) model of *Aeschbach-Hertig et al.* [2008]; l-step degassing (SD) model of *Brennwald et al.* [2003]), or as a diffusion dominated process (e.g., partial re-equilibration (PR) model of *Stute* [1989]; partial degassing (PD) model of *Stute et al.* [1995]). Here, we use inverse fitting procedures by *Ballentine and Hall* [1999] to fit NGTs, excess air and appropriate degassing parameters from measured noble gas concentrations for each of the 16 inconsistent samples at their sampling altitudes using the CE, SD, PR and PD models. Any particular model is assumed to explain the observed data set only if the χ^2 test between modeled and measured concentrations yields a probability $p > 0.01$ [see e.g., *Aeschbach-Hertig et al.*, 2008].

[39] Results of inverse fitting NGTs, excess air and fractionation parameter (F) for the CE model as well as NGTs and degassing volume, B for the SD model are provided in the auxiliary material. While only three (sc2-1, sz3-1 and sz4-1) out of the 16 samples satisfy the established χ^2 test probability ($p > 0.01$; χ^2 (1) = 6.63) using the CE model, three samples from San Cristobal (sc2-1, sc3-1, sc6-2) and two samples from Santa Cruz (sz3-1, sz4-1) satisfy the χ^2 test probability ($p > 0.01$; χ^2 (2) < 9.21) for the SD model. Three out of five samples that can be fit using the SD model (sc2-1, sc6-2, sz4-1) display either a greater depletion of the lighter noble gases relative to the heavier ones (sc2-1, sz4-1) or a greater depletion of the heavier noble gases relative to the lighter ones (sc6-2). Both patterns have previously been shown to be predicted by the CE model [*Aeschbach-Hertig et al.*, 2008]. However, solubility controlled models fail to achieve the established probability criteria ($p > 0.01$) for most inconsistent samples.

[40] Inverse fitting dissolved noble gas concentrations using the PR model show that only four out of 16 samples (sc3-1, sc3-2, sc5-2, sc10-2) converge to a global minimum with the non-negative excess air constraint in place. For samples that converge, best-fit χ^2 values result in poor fits (χ^2 (1) > 6.63). The PR model has been shown to require large amounts of initial dissolved excess air [*Kipfer et al.*, 2002], which is lacking in all our inconsistent samples and might thus explain the poor fits obtained. Inverse fitting using the alternate diffusion-based PD model shows that none of the 16 samples converge to a global minimum. Lack of convergence of these samples to a global minimum does not necessarily negate diffusion as the underlying process. Instead, it highlights the numerical instability of noble gas models with one degree of freedom [see e.g., *Ballentine and Hall*, 1999].

[41] Existing solubility and diffusion controlled degassing models tested in this study are only able to account for a small subset of all inconsistent samples. Both solubility and diffusion based degassing models favor the loss of lighter noble gases such as He and Ne over the heavier noble gases Kr and Xe. While diffusion based degassing models naturally favor the loss of Ne over Xe due to its higher diffusion coefficient, solubility based degassing models favor the loss of Ne over Xe due to Xe's greater solubility. Therefore, both solubility and diffusive degassing models are more likely to fit samples that display a progressive depletion of lighter noble gases as compared to the heavier ones or vice versa. By contrast, most of our samples (Figure 9a) display a unique depletion pattern with relative Ar excess compared to all other noble gases. Such patterns are possibly caused by processes unique to fractured environments, as investigated below. It is also relevant to note that our noble gas data, unlike data from active volcanic environments [e.g., *Gardner*, 2010] are not compatible with the presence of a hydrothermal gas phase, and thus, with the occurrence of a Rayleigh type of degassing that might lead to the observed pattern of our inconsistent samples. Indeed, only samples located at high altitude, which are referred here as "inconsistent" could possibly point to the presence of a mantle gas phase. However, if that were the case, all the "consistent" samples, which point to the presence of a closed system and absence of a gas phase, should also display the impact of a mantle gas phase, and this is not the case. Indeed, all consistent samples are located at low altitude and samples from the basal aquifer are "consistent," i.e., their signature is that expected for a closed system and thus, incompatible with the presence of a hydrothermal gas phase and possible occurrence of a Rayleigh degassing hypothesis.

7.2. Dissolution of Noble Gases in Fog Droplets

[42] As many as 14 out of 16 inconsistent water samples are located at high altitudes (>$\sim$420 m) where the presence of fog is prominent during the "garúa" season. Fog droplets generally form under conditions that significantly deviate from the standard noble gas assumption of equilibration at the unsaturated-water table interface at standard atmospheric pressure (Figure 10). Fog droplets suspended in oversaturated air represent an anisobaric system since water pressure within the droplet is greater than the surrounding atmospheric pressure ($P_{water} > P_{air}$) due to its curvature [*Mercury et al.*, 2003]. Due to this increase in water pressure within the droplet, noble gases will move from within the droplet to the surrounding air. Consequently, if infiltration of droplets is too fast so as to prevent re-equilibration of the droplets with the soil air at the water table, noble gas composition at recharge might reflect the particular metastable conditions under which these droplets formed. Although we do not expect the effect of curvature of fog droplets to independently explain the observed noble gas depletion pattern with relative Ar excess, a combination of this effect with other processes and in particular mixing with high-altitude rain is partially capable of reproducing the observed noble gas patterns as shown below. Thus, we

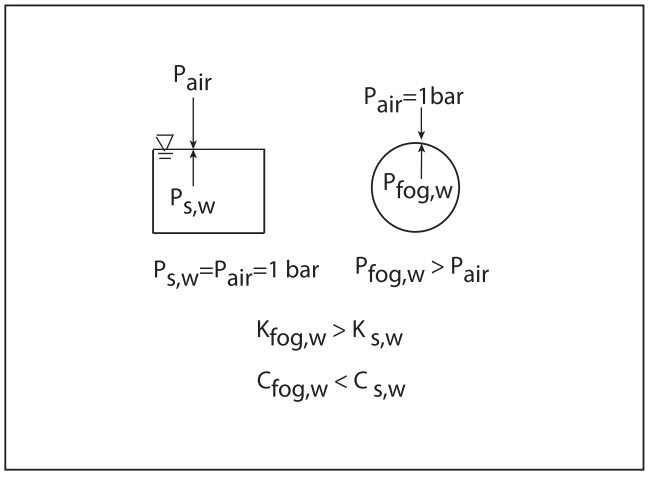

Figure 10. Comparison of noble gases within fog droplets and on a plane water surface (s, w). Water pressure within fog droplet, $P_{fog,w}$ is greater than atmospheric pressure P_{air} due to effect of curvature. Increased water pressure increases dimensionless Henry's constant, $K_{fog,w}$ for noble gases thereby decreasing dissolved noble gas concentrations within fog droplets, $C_{fog,w}$ as compared to plane surface water, $C_{s,w}$

first explore the sole effect of curvature on the dissolution of noble gases within fog droplets.

[43] Dissolution of noble gases in fog droplets was investigated using a framework described by *Mercury et al.* [2004] for positive pressure values of droplet curvature. The increase in water pressure due to curvature of the droplet can be calculated using the Laplace equation of capillarity and the Kelvin equation [*Thomson*, 1871]. An increase in water pressure, *dP*, decreases the solubility of the noble gas considered through a modification of its Henry's constant k_i. This decrease in solubility of the noble gas '*i*' at constant temperature '*T*' is given by [*Mercury et al.*, 2004]:

$$\ln \frac{k_i(T,P)}{k_i(T,1)} = \frac{1}{RT} \int_1^P V^0_{\text{solute}} \bullet dP, \tag{3}$$

where *R* is the universal gas constant and V^0_{solute} is the volume of noble gas '*i*' in solution [*Mercury et al.*, 2003], which can be calculated using thermodynamic constants in the work of *Mercury et al.* [2004] (additional details for this calculation are provided in the auxiliary material). The effect of changing pressure on noble gas solubility was incorporated into a UA model framework [cf. *Ballentine and Hall*, 1999] to calculate NGTs and excess air (constrained by nonnegativity) for different assumed recharge altitudes, from the sampling altitude up to 3000 m with 50 m increments, and positive water pressures corresponding to droplet sizes of 0.3, 1 and 10 microns. These droplet sizes represent the theoretical diameter of aerosols that can be activated to become fog droplets (see auxiliary material for a discussion on droplet sizes) for a typical maximum supersaturation of 0.1% observed in fog in the Galapagos Islands [cf., *Seinfeld and Pandis*, 2006; *Collins and Bush*, 2010]. The validity of the model at a specific altitude and droplet size is evaluated through a chi-square (χ^2) test. The model is assumed to explain the observed data set only if the χ^2 test yields a probability $p > 0.01$ (χ^2 (2) < 9.2) at that specific altitude and droplet size [*Aeschbach-Hertig et al.*, 2008].

[44] Minimum recharge altitudes obtained for all 16 inconsistent samples using different droplet sizes with nonnegative excess air constraint and $\chi^2 < 9.2$ are higher than the peak altitude of the islands. However, for samples with $\chi^2 < 9.2$, minimum recharge altitudes obtained through this model were lower by up to 50 m for a 1 micron droplet as compared to the minimum recharge altitudes obtained using the UA model and thus, move altitudes in the expected direction. NGTs obtained through this model, however, are not significantly different.

[45] Although these results are encouraging as they bring some of our samples closer to the expected altitudes and temperatures, it can be concluded that the magnitude of the effect of curvature based on the chosen size of fog droplets is, by itself, insufficient to explain the observed depletion of noble gas pattern in the inconsistent samples. Below, we discuss in more detail our proposed hypothesis of mixing between high-altitude rainwater and fog droplets to account for the pattern of the 11 inconsistent samples that cannot be explained by existing solubility and diffusion controlled degassing models.

7.3. Effect of Mixing High-Altitude Rainwater With Low-Altitude Fog Droplets

[46] Apparent high-recharge altitudes and cold temperatures displayed by many samples (cf. section 4.2) suggest that the available time for rainwater to re-equilibrate with the soil air of the islands might be insufficient due to rapid water infiltration through fractures commonly seen in basaltic settings. Figure 11 shows the 11 inconsistent Galapagos samples (yellow circles) along with measured noble gases in rainfall (green circles) and theoretical (modeled) fog concentration (blue square) plotted as F(Xe) versus F(Ne) where $F(i) = ([i]/[Ar])_{sample}/([i]/[Ar]_{asw})$, "i" represents any noble gas and "asw" is the air saturated water value at 20°C. Such a plot of F(Xe) versus F(Ne) is commonly used to study noble gas fractionation patterns in groundwater [e.g., *Kennedy et al.*, 1985; *Gardner et al.*, 2010]. Rain samples were collected in Michigan (cf. auxiliary material) while the fog droplet concentration is the expected theoretical concentration corresponding to a droplet size of 10 microns at 20°C (cf. section 7.2). Also shown are theoretical values for ASW at different temperatures (solid line) along with expected patterns for Rayleigh degassing [*Porcelli et al.*, 2002] at different temperatures (dashed lines). Comparison of rainfall in Michigan and ASW values (Figure 11) shows that noble gases in rainfall deviate from expected ASW values. In particular, the rainwater samples show noble gas patterns similar to a Rayleigh style degassing at temperatures of approximately 16°C and 34°C, temperatures far higher than the measured surface air temperatures of 10°C and 25°C at the time of their respective sample collection. Similar deviations of measured noble gas concentrations in rainfall with respect to surface conditions were previously observed in the Jordan Rift Valley [*Mazor*, 1972]. Although the nature of

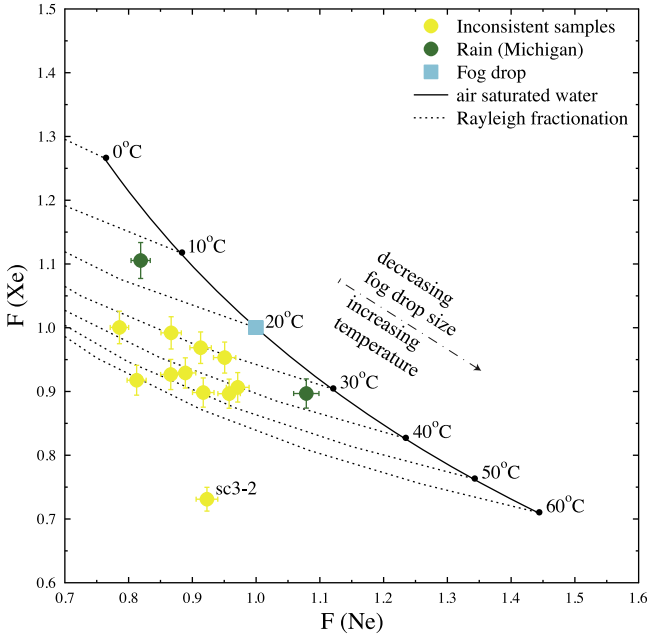

Figure 11. F(Xe) versus F(Ne) for 11 inconsistent Galapagos samples (yellow circles) along with measured rain (green circles) and theoretical fog droplet (blue square) concentration at 20°C and 10 micron size. Also shown are values for air saturated water (solid line) and expected Rayleigh style degassing pattern (dashed line) at different temperatures. Rain samples indicate Rayleigh style degassing at higher temperatures while decreasing fog droplet size is expected to correspond to apparent increase in temperature.

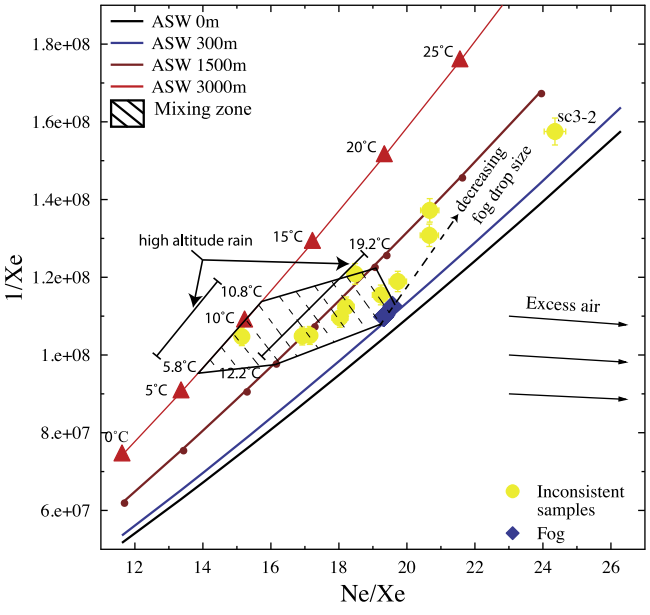

Figure 12. 1/Xe versus Ne/Xe for 11 inconsistent Galapagos samples (yellow circles) along with high-altitude rainwater and theoretical fog concentrations (blue diamonds) for drop sizes at 0.3, 1 and 10 microns at 421 m and 20°C. Decreasing fog drop size corresponds to an apparent increase in altitude and temperature. Zone of mixing between high-altitude rainwater and fog droplets is indicated by the shaded region.

this deviation remains poorly understood, it is apparent that rainwater, independent of geographic location, is not always in equilibrium with ground surface conditions.

[47] In addition to the deviation of rainfall from expected ASW values, fog droplets suspended in oversaturated air are expected to contain lower dissolved noble gases compared to ASW at similar altitudes and temperatures (section 7.2). Noble gas solubility within fog droplets decreases with fog droplet size in a nonlinear fashion (equation (3), section 7.2). Because of decreased noble gas solubility within the fog droplet, noble gases point to an apparent increase in temperature (dashed arrow line, Figure 11) and altitude (shown below) as compared to ASW values. It is thus apparent that both fog droplets and rainwater are not in equilibrium with ground surface conditions and it is possible that mixing between these two components might reproduce the noble gas pattern observed in these 11 inconsistent Galapagos samples as discussed below.

[48] Figure 12 shows 1/Xe versus Ne/Xe for 11 inconsistent Galapagos samples (yellow circles) along with rainwater equilibrated at different altitudes and temperatures mixing with fog droplets of 0.3, 1 and 10 microns at 421m and 20°C. Condensation altitudes and temperatures during the hot season were obtained by analyzing radio sonde measured dew point differences at different elevations between 1967 and 2010 for San Cristobal (see http://www.ncdc.noaa.gov/oa/climate/igra/). Condensation (dew point difference <0.5°C) occurs mostly at elevations of 850 mbar ($\sim$1500 m asl) and 700 mbar ($\sim$3100 m) at temperatures between 12.2 and 19.2°C and 5.8 and 10.8°C, respectively. Mixing between rainwater that equilibrated at high altitudes and fog droplets of various droplet sizes will produce a mixture that is different in composition from either source (shaded region, Figure 12). As many as seven out of eleven inconsistent samples (yellow circles) fall within this zone of mixing and have thus, the potential to explain the observed noble gas patterns in these samples. Three samples that fall outside of the shaded area (excluding sc3-2 which underwent evaporation, cf. section 5.2) would require fog droplet sizes <0.3 microns. Because currently measured fog droplet sizes are ≥ 0.1 microns (see auxiliary material), these three samples are not considered in the analysis below. Because Figure 12 can evaluate only two (Ne, Xe) out of four (Ne, Ar, Kr, Xe) measured noble gases, below, we evaluate, through a statistical analysis, the mixing hypothesis using all four noble gases simultaneously for the 7 inconsistent samples located within the shaded mixing area (Figure 12), assuming high-altitude rainfall and fog droplet end members as discussed above.

[49] High-altitude rainwater was mixed in different proportions (0–100%) with fog water of varying droplet size (0.3, 1, 10 micron) at an average elevation of 400 m and a mean temperature of 19.4°C extrapolated from measured mean "garúa" temperature at Puerto Ayora using a gradient of -0.8°C/100 m. For each of the above combinations, χ^2 values were calculated as the sum of the ratio of the squared concentration differences between measured and hypothetical noble gas mixture for all four noble gases, divided by their respective squared measurement uncertainties. For each of the 7 inconsistent samples, a best mixing

combination was then identified as the mixture combination with the least χ^2 value. Minimum χ^2 values thus found for many samples after mixing were lower than those for either end members. Minimum χ^2 values obtained through this mixing hypothesis also show a significant improvement over the constrained CE ($0 < F < 1$) and UA models. However, a χ^2 test ($p < 0.01$; $\chi^2(4) = 13.28$) considered simultaneously for all four noble gases for this hypothesis is unsuccessful.

[50] Although our mixing hypothesis is capable of explaining Ne and Xe concentrations for all 7 samples (Figure 12), our statistical analysis based simultaneously on all four noble gases is unsuccessful. This suggests that our model parameter estimates for either end members may not be accurate. Among these are condensation altitudes and temperatures, as well as initial fog equilibration conditions. Measurements of noble gases in fog are currently nonexistent and are very scarce in rainfall [*Mazor*, 1972; this study]. Such measurements together with measurement of rates of noble gas equilibration during surface runoff and within fractures should provide better constraints on the above model parameters and need to be carried out in future studies.

8. Conclusions

[51] NGTs are successfully used to identify recharge areas and timing of recharge in basal and perched aquifers in the fractured, baslatic hydrologic systems of Santa Cruz and San Cristobal in the Galapagos Archipelago. Specifically, recharge altitudes between 160 and 870 m and temperatures between 20.05 ± 2.07°C and 27.54 ± 0.47°C are found for the basal aquifer in Santa Cruz, while recharge altitudes between 229 and 730 m and temperatures of 19.95 ± 1.13°C and 26.36 ± 0.66°C are found for springs in San Cristobal. Timing of recharge obtained through NGTs for all samples are also corroborated by stable isotope results. Except for one sample, combined NGT and stable isotope analyses points to recharge during the hot season for all low-altitude (<∼420 m) spring samples from San Cristobal and all basal aquifer samples in Santa Cruz. Stable isotope analyses also indicate that San Cristobal springs located at high altitudes (>420 m asl) are recharged during both the "garúa" and hot seasons. These results suggest that the composition of recharge water at different altitudes follows the distribution of rainfall closely, as previously suggested for Santa Cruz [*d'Ozouville et al.*, 2008a]. Robust agreement on timing of recharge between NGTs and stable isotopes also suggests that seasonal variations in temperature are likely to be preserved by noble gases dissolved in groundwater in basaltic environments in the presence of fractures or where soil cover is thin. Groundwater residence times for all springs derived from measured R/R_a values and tritium content in precipitation all yield young ages (<11 ± 4.5 years) and further reinforce the notion that NGTs and stable isotopes in this system are indeed recording seasonality as opposed to the commonly assumed MAAT in sedimentary systems.

[52] Samples located at high-altitude (>∼420 m) display systematic deviations of dissolved noble gases from expected ASW values and lead to equilibration recharge altitudes and temperature conditions that are not consistent with conditions on the ground using standard NGT models. Most inconsistent samples indicate a unique noble gas pattern with relative Ar excess together with a strong depletion of Ne, Kr and Xe. Existing degassing models are only able to account for the observed noble gas pattern for 5 out of 16 inconsistent samples. The impact of fog droplets ("garúa" dew) on dissolved noble gas concentrations in groundwater on the highlands was explored. Although the effect of fog droplets brings some inconsistent samples closer to the expected altitudes and temperatures, such mechanism, by itself, is insufficient to reproduce the observed noble gas patterns. On the other hand, the effect of mixing high-altitude atmosphere rainwater with fog droplets is capable of explaining Ne and Xe concentrations for many of the inconsistent samples. However, a statistical analysis conducted of the mixing hypothesis based simultaneously on all four noble gases is unsuccessful, and suggests that our model parameter estimates are ill constrained. A full understanding of this unique noble gas signature is out of the scope of this study and will be the object of future investigations.

Appendix A

[53] Extreme temperature value transects were computed by combining available weather data measured using weather balloons and land stations during the hottest month (March) in an El Nino (1992) year and during the coldest month (September) in a La Nina (2007) year for each of the islands. Weather balloons are launched at sea level daily at 6am in San Cristobal and measure air temperatures at different elevations (these compare well with minimum surface temperature measurements observed at the land station in Puerto Bacquerizo Moreno (7.9 m asl); see http://www7.ncdc.noaa.gov/CDO/cdo). Because weather balloons record only minimum temperatures, the extreme maximum temperature-altitude transect (Figure 5, red dashed line) is calculated based on maximum diurnal temperature variations computed from available land station data. Because weather records on diurnal temperature variation during the hottest month (March) in the El Nino (1992) year are unavailable, extreme maximum temperatures in San Cristobal were calculated by combining weather balloon data for March 1992 (see http://www.ncdc.noaa.gov/oa/climate/igra/) with the mean monthly observed diurnal temperature variation (±7.15°C) for the closest available diurnal temperature data set (March, 1993) (see http://www7.ncdc.noaa.gov/CDO/cdo). Extreme minimum temperatures (Figure 5, blue dashed line) in San Cristobal are those of weather balloon temperatures (always recorded at 1200 UTC [i.e., 0600 local Galapagos time (GALT)] see http://www.ncdc.noaa.gov/oa/climate/igra/) for the coldest month (September) in a La Nina year (2007). Maximum and minimum temperatures recorded for weather stations in Puerto Ayora and Bellavista for the same extreme events (see http://www.darwinfoundation.org/datazone/darwin_weather) were used along with the established annual temperature gradient (−0.8°C/100 m) [*Auken et al.*, 2009] to estimate extreme maximum and minimum temperature transects in Santa Cruz.

[54] **Acknowledgments.** We thank Selker J. and the Associate Editor for the editorial handling of this manuscript, as well as three anonymous reviewers for their insightful and thorough reviews. We thank Noémi

d'Ozouville and Sophie Violette for field sampling and logistics with local authorities through the Galapagos Islands Integrated Water Studies project. We are also thankful to the Galapagos National Park Service, the Charles Darwin Foundation, the Municipalities of Santa Cruz and San Cristobal, and the Galapagos National Institute for local collaboration and logistics. Financial support by the National Geographic Society award 8452-08 and the National Science Foundation CAREER award EAR-0545071 is greatly appreciated.

References

Adelinet, M., J. Fortin, N. d'Ozouville, and S. Violette (2008), The relationship between hydrodynamic properties and weathering of soils derived from volcanic rocks, Galapagos Islands (Ecuador), *Environ. Geol.*, *56*, 45–58.

Aeschbach-Hertig, W., F. Peeters, U. Beyerle, and R. Kipfer (1999), Interpretation of dissolved atmospheric noble gases in natural waters, *Water Resour. Res.*, *35*, 2779–2792.

Aeschbach-Hertig, W., F. Peeters, U. Beyerle, and R. Kipfer (2000), Paleotemperature reconstruction from noble gases in ground water taking into account equilibration with entrapped air, *Nature*, *405*, 1040–1044.

Aeschbach-Hertig, W., H. El-Gamal, M. Wieser, and L. Palcsu (2008), Modeling excess air and degassing in groundwater by equilibrium partitioning with a gas phase, *Water Resour. Res.*, *44*, W08449, doi:10.1029/2007WR006454.

Amos, R. T., K. U. Mayer, B. A. Bekins, G. N. Delin, and R. L. Williams (2005), Use of dissolved and vapor-phase gases to investigate methanogenic degradation of petroleum hydrocarbon contamination in the subsurface, *Water Resour. Res.*, *41*, W02001, doi:10.1029/2004WR003433.

Andrews, J. N., and D. J. Lee (1979), Inert gases in ground water from the Bunter Sandstone of England as indicators of age and palaeoclimatic trends, *J. Hydrol.*, *41*, 233–252.

Andrews, J. N., I. S. Giles, R. L. F. Kay, D. J. Lee, J. K. Osmond, J. B. Cowart, P. Fritz, J. F. Barker, and J. Gale (1982), Radioelements, radiogenic helium and age relationships for groundwaters from the granites at Stripa, Sweden, *Geochim. Cosmochim. Acta*, *46*, 1533–1543.

Auken, E., S. Violette, N. d'Ozouville, B. Deffontaines, K. I. Sørensen, A. Viezzoli, and G. de Marsily (2009), An integrated study of the hydrogeology of volcanic islands using helicopter borne transient electromagnetic: Application in the Galápagos Archipelago, *C. R. Geosci.*, *341*, 899–907.

Ballentine, C. J., and C. M. Hall (1999), Determining paleotemperature and other variables using noble gas concentrations in water, *Geochim. Cosmochim. Acta*,, *63*, 2315–2336.

Bethke, C. M., X. Zhao, and T. Torgersen (1999), Groundwater flow and the 4He distribution in the Great Artesian Basin of Australia, *J. Geophys. Res.*, *104*, 12,999–13,011.

Bottomley, D. J., J. D. Ross, and W. B. Clarke (1984), Helium and neon isotope geochemistry of some ground waters from the Canadian Precambrian Shield, *Geochim. Cosmochim. Acta*, *48*, 1973–1985.

Brennwald, M. S., M. Hofer, F. Peeters, W. Aeschbach-Hertig, K. Strassmann, R. Kipfer, and D. M. Imboden (2003), Analysis of dissolved noble gases in the pore water of lacustrine sediments, *Limnol. Oceanogr.*, *1*, 51–62.

Castro, M. C. (2004), Helium sources in passive margin aquifers—New evidence for a significant mantle ^{3}He source in aquifers with unexpectedly low in situ ^{3}He/^{4}He production, *Earth Planet. Sci. Lett.*, *222*, 897–913.

Castro, M. C., A. Jambon, G. de Marsily, and P. Schlosser (1998a), Noble gases as natural tracers of water circulation in the Paris Basin. 1. Measurements and discussion of their origin and mechanisms of vertical transport in the basin, *Water Resour. Res.*, *34*, 2443–2466.

Castro, M. C., P. Goblet, E. Ledoux, S. Violette, and G. de Marsily (1998b), Noble gases as natural tracers of water circulation in the Paris Basin. 2. Calibration of a groundwater flow model using noble gas isotope data, *Water Resour. Res. 34*, 2467–2483.

Castro, M. C., M. Stute, and P. Schlosser (2000), Comparison of ^{4}He ages and ^{14}C ages in simple aquifer systems: implications for groundwater flow and chronologies, *Appl. Geochem.*, *15*, 1137–1167.

Castro, M. C., D. Patriarche, and P. Goblet (2005), 2-D numerical simulations of groundwater flow, heat transfer and ^{4}He transport—Implications for the He terrestrial budget and the mantle helium-heat imbalance, *Earth Planet. Sci. Lett.*, *237*, 893–910.

Castro, M. C., C. M. Hall, D. Patriarche, P. Goblet, and B. R. Ellis (2007), A new noble gas paleoclimate record in Texas—Basic assumptions revisited, *Earth Planet. Sci. Lett.*, *257*, 170–187.

Castro, M. C., L. Ma, and C. M. Hall (2009), A primordial, solar He-Ne signature in crustal fluids of a stable continental region, *Earth Planet. Sci. Lett.*, *279*, 174–184.

Cey, B. D., G. B. Hudson, J. E. Moran, and B. R. Scanlon (2008), Impact of Artificial Recharge on Dissolved Noble Gases in Groundwater in California, *Environ. Sci. Technol.*, *42*, 1017–1023.

Cey, B. D., G. B. Hudson, J. E. Moran, and B. R. Scanlon (2009), Evaluation of Noble Gas Recharge Temperatures in a Shallow Unconfined Aquifer, *Ground Water*, *47*, 646–659.

Clarke, W. B., W. Jenkins, and Z. Top (1976), Determinations of tritium by mass-spectrometric measurement of ^{3}He, *Int. J. Appl. Radiat. Isot.*, *27*(9), 515–522.

Collins, A., and M. B. Bush (2010), An analysis of modern pollen representation and climatic conditions on the Galápagos Islands, *Holocene*, *21*, 231–250.

Craig, H. (1961), Isotopic variations in meteoric waters, *Science*, *133*, 1702–1703.

Dansgaard, W. (1964), Stable isotopes in precipitation, *Tellus*, *16*, 436–468.

d'Ozouville, N. (2007), Étude du fonctionnement hydrologique dans les îles Galápagos: Caractérisation d'un milieu volcanique insulaire et préalable à la gestion de la ressource, PhD thesis, Université Pierre et Marie Curie, France, 474 pp.

d'Ozouville, N., E. Auken, K. Sorensen, S. Violette, G. de Marsily, B. Deffontaines, and G. Merlen (2008a), Extensive perched aquifer and structural implications revealed by 3D resistivity mapping in a Galapagos volcano, *Earth Planet. Sci. Lett.*, *269*, 518–522.

d'Ozouville, N., B. Deffontaines, J. Benveniste, U. Wegmüller, S. Violette, and G. de Marsily (2008b), DEM generation using ASAR (ENVISAT) for addressing the lack of freshwater ecosystems management, Santa Cruz Island, Galapagos, *Remote Sensing Environ.*, *112*, 4131–4147.

Dominguez, C., A. Pryet, P. Fuente-Tomai, S. Violette, M. Villacís, and N. d'Ozouville (2011), Fog interception and redistribution of rainfall by vegetation as controlling factors of recharge rates: A case-study in Galápagos Islands, *Geophys. Res. Abstr.*, *13*, EGU2011-2683-2.

Farley, K. A., and E. Neroda (1998), Noble gases in the Earth's mantle, *Annu. Rev. Earth Planet. Sci. Lett.*, *26*, 189–218.

Gardner, W. P., D. D. Susong, D. K. Solomon, and H. P. Heasler (2010), Using noble gases measured in spring discharge to trace hydrothermal processes in the Norris Geyser Basin, Yellowstone National Park, U.S.A., *J. Volcanol. Geotherm. Res.*, *198*, 394–404.

Geist, D. J., A. R. McBirney, and R. A. Duncan (1986), Geology and petrogenesis of lavas from San Cristobal Island, Galapagos Archipelago, *Geol. Soc. Am. Bull.*, *97*, 555–566.

Geist, D. J., W. M. White, and A. R. Mcbirney (1988), Plume-asthenosphere mixing beneath the Galapagos archipelago, *Nature*, *333*, 657–660.

Gonfiantini, R., M.-A. Roche, J.-C. Olivry, J.-C. Fontes, and G. M. Zuppi (2001), The altitude effect on the isotopic composition of tropical rains, *Chem. Geol.*, *181*, 147–167.

Hall, C. M., M. C. Castro, K. C. Lohmann, and L. Ma (2005), Noble gases and stable isotopes in a shallow aquifer in southern Michigan: Implications for noble gas paleotemperature reconstructions for cool climates, *Geophys. Res. Lett.*, *32*, L18404, doi:10.1029/2005GL023582.

Heaton, T. H. E., and J. C. Vogel (1981), "Excess air" in groundwater, *J. Hydrol.*, *50*, 201–216.

Heilweil, V., D. Solomon, S. Gingerich, and I. Verstraeten (2009), Oxygen, hydrogen, and helium isotopes for investigating groundwater systems of the Cape Verde Islands, West Africa, *Hydrogeol. J.*, *17*, 1157–1174.

Herzberg, O., and E. Mazor (1979), Hydrological applications of noble gases and temperature measurements in underground water systems: Examples from Israel, *J. Hydrol.*, *41*, 217–231.

James, E. R., M. Manga, T. P. Rose, and G. B. Hudson (2000), The use of temperature and the isotopes of O, H, C, and noble gases to determine the pattern and spatial extent of groundwater flow, *J. Hydrol.*, *237*, 100–112.

Jean-Baptiste, P., P. Allard, R. Coutinho, T. Ferreira, E. Fourré, G. Queiroz, and J. L. Gaspar (2009), Helium isotopes in hydrothermal volcanic fluids of the Azores archipelago, *Earth Planet. Sci. Lett.*, *281*, 70–80.

Kennedy, B. M., M. A. Lynch, J. H. Reynolds, and S. P. Smith (1985), Intensive sampling of noble gases in fluids at Yellowstone: I. Early overview of the data; regional patterns, *Geochim. Cosmochim. Acta*, *49*, 1251–1261.

Kennedy, B. M., J. H. Reynolds, and S. P. Smith (1988), Noble gas geochemistry in thermal springs, *Geochim. Cosmochim. Acta*, *52*, 1919–1928.

Kipfer, R., W. Aeschbach-Hertig, F. Peeters, and M. Stute (2002), Noble Gases in Lakes and Ground Waters, *Rev. Mineral. Geochem.*, *47*, 615–700.

Klump, S., Y. Tomonaga, P. Kienzler, W. Kinzelbach, T. Baumann, D. M. Imboden, and R. Kipfer (2007), Field experiments yield new insights into gas exchange and excess air formation in natural porous media, *Geochim. Cosmochim. Acta*, *71*, 1385–1397.

Kramer, P., and J. Black (1970), Scientific and conservation, *Rep. 21*, Charles Darwin Res. Station, Galapagos, Ecuador.

Lippmann, J., M. Stute, T. Torgersen, D. P. Moser, J. A. Hall, L. Lin, M. Borcsik, R. E. S. Bellamy, and T. C. Onstott (2003), Dating ultra-deep mine waters with noble gases and 36Cl, Witwatersrand Basin, South Africa, *Geochim. Cosmochim. Acta*, *67*, 4597–4619.

Lowenstern, J. B., and S. Hurwitz (2008), Monitoring a supervolcano in repose: Heat and volatile flux at the Yellowstone Caldera, *Elements*, *4*, 35–40.

Ma, L., M. C. Castro, and C. M. Hall (2004), A late Pleistocene noble gas paleotemperature record in southern Michigan, *Geophys. Res. Lett.*, *31*, L23204, doi:10.1029/2004GL021766.

Manning, A. H., and D. K. Solomon (2003), Using noble gases to investigate mountain-front recharge, *J. Hydrol.*, *275*, 194–207.

Marty, B., V. Meynier, E. Nicolini, E. Griesshaber, and J. P. Toutain (1993), Geochemistry of gas emanations: A case study of the Reunion Hot Spot, Indian Ocean, *Appl. Geochem.*, *8*, 141–152.

Mazor, E. (1972), Paleotemperatures and other hydrological parameters deduced from noble gases dissolved in groundwaters; Jordan Rift Valley, Israel, *Geochim. Cosmochim. Acta*, *36*, 1321–1336.

Mazor, E. (1977), Geothermal tracing with atmospheric and radiogenic noble gases, *Geothermics*, *5*(1-4), 21–36.

Mazor, E., and R. O. Fournier (1973), More on noble gases in Yellowstone National Park hot waters, *Geochim. Cosmochim. Acta*, *37*, 515–525.

Mercury, L., M. Azaroual, H. Zeyen, and Y. Tardy (2003), Thermodynamic properties of solutions in metastable systems under negative or positive pressures, *Geochim. Cosmochim. Acta*, *67*, 1769–1785.

Mercury, L., D. L. Pinti, and H. Zeyen (2004), The effect of the negative pressure of capillary water on atmospheric noble gas solubility in ground water and palaeotemperature reconstruction, *Earth Planet. Sci. Lett.*, *223*, 147–161.

Peeters, F., U. Beyerle, W. Aeschbach-Hertig, J. Holocher, M. S. Brennwald, and R. Kipfer (2002), Improving noble gas based paleoclimate reconstruction and groundwater dating using 20Ne/22Ne ratios, *Geochim. Cosmochim. Acta*, *67*, 587–600.

Porcelli, D., C. J. Ballentine, and R. Wieler (2002), An overview of noble gas geochemistry and cosmochemistry, *Rev. Miner. Geochem.*, *47*, 1–19.

Proctor and Redfern International Limited (2003), Actualizacion del Estudio de Factibiliad del Sistema de Agua y Saneamiento de Puerto Ayora, Reporte Final, project report (PO-PPF-1172/0C-EC), Proctor and Redfern Int., Ltd., Don Mills, Ontario, Canada.

Saar, M. O., M. C. Castro, C. M. Hall, M. Manga, and T. P. Rose (2005), Quantifying magmatic, crustal, and atmospheric helium contributions to volcanic aquifers using all stable noble gases: Implications for magmatism and groundwater flow, *Geochem. Geophys. Geosyst.*, *6*, Q03008, doi:10.1029/2004GC000828.

Schlosser, P., M. Stute, H. Dörr, C. Sonntag, and K. O. Münnich (1988), Tritium/3He dating of shallow groundwater, *Earth Planet. Sci. Lett.*, *89*, 353–362.

Schlosser, P., M. Stute, C. Sonntag, and K. O. Münnich (1989), Tritiogenic ^{3}He in shallow groundwater, *Earth Planet. Sci. Lett.*, *94*, 245–256.

Scholl, M. A., S. E. Ingebritsen, C. J. Janik, and J. P. Kauahikaua (1996), Use of precipitation and groundwater isotopes to interpret regional hydrology on a tropical volcanic island: Kilauea volcano area, Hawaii, *Water Resour. Res.*, *32*, 3525–3538.

Scholl, M. A., S. B. Gingerich, and G. W. Tribble (2002), The influence of microclimates and fog on stable isotope signatures used in interpretation of regional hydrology: East Maui, Hawaii, *J. Hydrol.*, *264*, 170–184.

Seinfeld, J. H., and S. N. Pandis (2006), *Atmospheric Chemistry and Physics: From Air Pollution to Climate Change*, Wiley, Hoboken, N. J.

Stute, M. (1989), Edelgase im Grundwasser—Bestimmung von Paläotemperaturen und Untersuchung der Dynamik von Grundwasserfliesssystemen, PhD thesis, Univ. of Heidelberg, Heidelberg, Germany, 138 pp.

Stute, M., and P. Schlosser (1993), Principles and applications of the Noble gas paleothermometer, vol. 78, in *Climate Change in Continental Isotopic Recors*, Geophys. Monogr. Ser., edited by P. K. Swart et al., pp. 89–100, AGU, Washington, D. C.

Stute, M., and C. Sonntag (1992), Paleotempertures derived from noble gases dissolved in groundwater and in relation to soil temperature, in *Isotopes of Noble Gases as Tracers in Environmental Studies, Proceedings of a Consultants Meeting on Isotopes of Noble Gases as Tracers in Environmental Studies*, p. 305, Int. At. Energy Agency, Vienna.

Stute, M., P. Schlosser, J. F. Clark, and W. S. Broecker (1992), Paleotemperatures in the southwestern United States derived from Noble Gases in ground water, *Science*, *256*, 1000–1003.

Stute, M., M. Forster, H. Frischkorn, A. Serejo, J. F. Clark, P. Schlosser, W. S. Broecker, and G. Bonani (1995), Cooling of tropical Brazil (5°C) during the last glacial maximum, *Science*, *269*, 379–383.

Sun, T., C. M. Hall, M. C. Castro, K. C. Lohmann, and P. Goblet (2008), Excess air in the noble gas groundwater paleothermometer: A new model based on diffusion in the gas phase, *Geophys. Res. Lett.*, *35*, L19401, doi:10.1029/2008GL035018.

Sun, T., C. M. Hall, and M. C. Castro (2010), Statistical properties of groundwater noble gas paleoclimate models: Are they robust and unbiased estimators?, *Geochem. Geophys. Geosyst.*, *11*, Q02002, doi:10.1029/2009GC002717.

Thoma, M. J., J. P. McNamara, M. M. Gribb, and S. G. Benner (2011), Seasonal recharge components in an urban/agricultural mountain front aquifer system using noble gas thermometry, *J. Hydrol.*, *409*, 118–127.

Thomson, W. (1871), On the equilibrium of vapor at a curved surface of liquid, *Philos. Mag.*, *42*, 448–452.

Torgersen, T., and G. N. Ivey (1985), Helium accumulation in ground water, *II*: A model for the accumulation of the crustal 4He degassing flux, *Geochim. Cosmochim. Acta*, *49*, 2445–2452.

Trueman, M., and N. d'Ozouville (2010), Characterizing the Galapagos terrestrial climate 1965–2009: A baseline for comparing future possible climate change, *Galapagos Res.*, *67*, 26–37.

Visser, A., H. P. Broers, and M. F. P. Bierkens (2007), Dating degassed groundwater with 3H/3He, *Water Resour. Res.*, *43*, W10434, doi:10.1029/2006WR005847.

Weiss, R. F. (1968), Piggyback sampler for dissolved gas studies on sealed water samples, *Deep Sea Res. Oceanogr. Abstr.*, *15*, 695–699.

White, M. W., A. R. McBirney, and R. A. Duncan (1993), Petrology and geochemistry of the Galapagos Islands: Portrait of a pathological mantle plume, *J. Geophys. Res.*, *98*(B11), 19,533–19,563, doi:10.1029/93JB02018.

M. C. Castro, C. M. Hall, and R. B. Warrier, Department of Earth and Environmental Sciences, University of Michigan, 1100 N. University Ave., MI 48109-1063, Ann Arbor, USA. (mccastro@umich.edu; cmhall@umich.edu; warrierr@umich.edu)